Measurement 239 (2025) 115466



Contents lists available at ScienceDirect

Measurement

journal homepage: www.elsevier.com/locate/measurement





# Validation of the GUM uncertainty framework and the Unscented transformation for Brewer UV irradiance measurements using the Monte Carlo method

Carmen González [a,b,*], José M. Vilaplana [a], Francisco C. Parra-Rojas [c,d], Antonio Serrano [b]

[a] Área de Investigación e Instrumentación Atmosférica, Instituto Nacional de Técnica Aeroespacial (INTA), El Arenosillo, Huelva, Spain
[b] Departamento de Física, Instituto del Agua, Cambio Climático y Sostenibilidad, Facultad de Ciencias, Universidad de Extremadura, Badajoz, Spain
[c] Departamento de Ciencias Naturales y Matemáticas, Universidad Interamericana de Puerto Rico, Campus Bayamón, Puerto Rico, USA
[d] Centro de Investigación Atmosférica de Izaña, Agencia Estatal de Meteorología, Santa Cruz de Tenerife, Spain

ARTICLE INFO

*Keywords:*
Ultraviolet irradiance
Uncertainty
Monte Carlo
GUM
Unscented transformation
Brewer spectrometer

ABSTRACT

The uncertainty evaluation of spectral ultraviolet (UV) irradiance measurements is usually performed following the recommendations set by the GUM, the standard for uncertainty evaluation in metrology. In particular, the GUM uncertainty framework (GUF) is applied. Due to the difficulties in the propagation of uncertainties, it is standard practice to neglect the non-linearity of the irradiance model. To verify this assumption, the GUF is validated using the Monte Carlo method (MCM), as recommended by the GUM. As an alternative to these methods, an Unscented transformation (UT) has also been implemented and validated with the MCM. The data used are the UV scans recorded by a Brewer MKIII spectroradiometer at El Arenosillo Observatory. Evaluation of the spectral ratios between the combined standard uncertainties provided by the GUF, the UT, and the MCM showed that the agreement between the three methodologies is satisfactory.

## 1. Introduction

Ultraviolet (UV) radiation covers the shortest wavelengths of the incident solar spectrum, from 280 to 400 nm. This radiation is known for both its beneficial and adverse effects on living organisms, such as humans [1,2], animals [3,4], plants [5–7], or microorganisms [8–10]. Due to the inverse relationship between the amount of total ozone and associated changes in surface UV levels, UV data has been used traditionally to monitor the ozone layer and to evaluate the impact of the ozone depletion on surface UV levels and the ecosystem (e.g. [11–14]). In particular, spectral measurements are needed to accurately monitor these effects, since the energy of photons increases as wavelength decreases. However, spectral UV measurements also contain information about other atmosphere parameters, such as aerosols [15,16], clouds [17,18], or trace gases [19,20]. Therefore, spectral UV data can be used in numerous kinds of research, such as trend detection, climate change studies, calculation of UV doses for different biological action spectra, validation of radiative transfer models, etc. However, the measurement of spectral UV irradiance is a demanding task, requiring well-characterised and precise spectroradiometers to detect the possible changes in surface UV levels.

The characterisation of spectroradiometers as well as the quality of their UV measurements are determined by QA (quality assurance) and QC (quality control) procedures. QA is well established and evaluates the instrument's performance, typically through intercomparison campaigns [21–23]. On the other hand, QC involves the assessment of the uncertainty of measurements by characterising and identifying the uncertainty sources affecting the instrument. Ideally, a quality control system should have been established before the monitoring networks were operating. Unfortunately, this is not the case for UV. As a result, no standard QC practices were defined and UV measurements were habitually reported without their corresponding uncertainty, an estimation needed to indicate their quality and ensure their comparability to other measurements [24]. To overcome this limitation, several guides have been developed for the uncertainty evaluation of spectroradiometers following the general rules set by the Guide to the Expression of Uncertainty in Measurement (GUM) [25–27]. The standard methodology consists in applying the GUM uncertainty framework (hereafter "GUF") [28–31]. This method describes the uncertainty sources using their expectation and standard deviation as the best estimate and standard

* Corresponding author at: Área de Investigación e Instrumentación Atmosférica, Instituto Nacional de Técnica Aeroespacial (INTA), El Arenosillo, Huelva, Spain.
*E-mail address:* carmengh@unex.es (C. González).

https://doi.org/10.1016/j.measurement.2024.115466
Received 5 May 2024; Received in revised form 22 July 2024; Accepted 5 August 2024
Available online 8 August 2024
0263-2241/© 2024 The Author(s). Published by Elsevier Ltd. This is an open access article under the CC BY license (http://creativecommons.org/licenses/by/4.0/).

uncertainty, respectively. The uncertainty of the UV irradiance is then obtained by propagating the previous information using the law of propagation of uncertainty (LPU).

Applying the LPU requires the calculation of the partial derivatives of the model [24]. For UV spectroradiometers this is a challenging task as the model used to derive irradiance is complex (e.g. [29,32], formed by a set of equations and processing software, thus complicating the partial derivation. Furthermore, for a correct propagation of the uncertainty, a detailed characterisation and deep knowledge of the instrument are needed. Consequently, thorough uncertainty studies for spectral UV measurements are scarce [25,28,33]. Bais [34] and Bernhard and Seckmeyer [25] have reviewed the main uncertainty sources affecting UV spectroradiometers. However, in an effort to simplify the uncertainty evaluation, the standard practice is to disregard the non-linearity of the irradiance model [25,28,29,35,36]. This assumption as well as the conditions needed for the application of the GUF have not been validated and, as a result, uncertainties estimated in this way could be incorrect.

The limitations of the GUF are well-known and several approaches have been developed to provide reliable estimations for non-linear systems, such as the Unscented transformation (hereafter "UT") or the Monte Carlo method (hereafter "MCM"). Both techniques are numerical and do not rely on the calculation of the partial derivatives of the model. The MCM has a broader domain of validity [37], but depending on the number of parameters and sample points its computational complexity can be very high. On the other hand, the UT is a widely used algorithm for predicting means and covariances by propagating a small set of carefully chosen sample points (referred to as sigma points). It is accurate to at least the second order [38] and computationally less expensive than the MCM. Although the UT is a powerful tool for uncertainty analysis [39–43], to the best knowledge of the authors, it has never been used for the uncertainty evaluation of spectral UV irradiance measurements.

Thus, the original contribution of this paper is the validation of the GUF (assuming liner effects and uncorrelated sources) and the UT for solar UV measurements by comparing its results to those of the MCM. This comparison is recommended by the GUM, as the MCM has a broader domain of validity and accounts for non-linear effects and correlations in the data [37,44]. The uncertainty analysis carried out with the GUF and the UT led to similar results to those of the MCM as the mean relative difference between the two methods and the MCM was less than 1.5 % for all wavelengths and SZAs below 65°. The spectral UV measurements used were recorded by Brewer MKIII #150 spectrophotometer during the XVI international comparison campaign of the Regional Brewer Calibration Center – Europe (RBCC-E) at El Arenosillo in Huelva, Spain.

The article is organised as follows. First, the technical characteristics of the Brewer spectrophotometer are described in Sect. 2. Next, Sect. 3 presents the irradiance measurement model, the uncertainty sources as well as the GUF, UT, and MCM methods for uncertainty evaluation. Then, in Sect. 4 the results obtained from the GUF and UT validation against the MCM are discussed. Finally, Sect. 5 summarises the main conclusions of this study.

## 2. Instrumentation and site

The spectral measurements of solar UV irradiance used in this work were recorded by a double-monochromator Brewer (type MKIII, with serial number 150) spectrophotometer (hereafter "Brewer #150"). This instrument has been measuring total ozone column (TOC), global UV spectral irradiance, and aerosol optical depth (AOD) since 1997. In fact, its UV time series has been used in many studies, thus this spectrometer has served the scientific community monitoring UV for more than 20 years [33,45–53].

Brewer #150 measures spectral UV irradiance from 290 to 363 nm, with a nominal step of 0.5 nm. The shape of its slit function is triangular, and the Full Width Half Maximum (FWHM) is 0.55 nm. With these settings, a complete scanning of a UV spectrum takes 4.5 min. In 2005, the traditional entrance optics (a flat diffuser) was replaced by the UV-J1015 optic from CMS-Schreder. This entrance optic is designed to reduce the cosine error of the instrument, improving in turn the quality of global UV irradiance measurements [54]. Regarding the spectrometer, it is a modified Elbert type and consists of two monochromators and a slit mask located in front of the exit slit plane. The double monochromator is arranged so that the stray light of the system is greatly reduced [55]. A diagram of the optical assemblies of a Brewer MKIII spectrophotometer can be found in González et al. [33].

To ensure the quality of Brewer #150 UV measurements, the instrument is calibrated yearly following the standard procedure. It consists of measuring the irradiance emitted by several 1000 W tungsten lamps that are placed on top of the instrument's diffuser. The uncertainty of this calibration procedure is mainly produced by errors in the distance adjustment, the current, and the spectral irradiance emitted by the reference lamps. Furthermore, Brewer #150 also participates biannually in intercomparison campaigns, where its performance is validated against the European portable reference QASUME [35,56] from the Physikalisch-Meteorologisches Observatorium Davos / World Radiation Center. All these calibration procedures result in uncertainties of 3–4 % [33].

Brewer #150 is located on the roof of the El Arenosillo Atmospheric Sounding Station of the National Institute of Aerospace Technology (INTA) in Huelva, Spain (37.1°N, 6.7°W, 41 m above sea level). The horizon of the instrument's entrance optic is free up to a solar zenith angle (SZA) of 85°. Furthermore, the station is surrounded by pine forest, which results in a uniform surface albedo. All these conditions, alongside the high number of cloud-free days per year, makes "El Arenosillo" a suitable site for reliable radiometric measurements. In fact, since 2003, this station hosts every two years the RBCC-E international calibration campaigns, where Brewer and, more recently, CCD-array spectroradiometers are calibrated for TOC and spectral UV irradiance.

## 3. Methodology

The data used for this study correspond to the UV measurements performed by Brewer #150 from 10 to 15 September 2021, during the XVI Intercomparison campaign of the RBCC-E held at "El Arenosillo" Observatory. Only cloud-free scans have been considered in order to obtain reliable uncertainty estimations. Brewer spectrophotometers take a considerable amount of time to perform a UV scan and, as a result, are unable to detect the fast changes clouds can have on surface UV radiation.

In this work, the combined standard uncertainty of Brewer UV measurements as well as the uncertainties arising from every error source have been determined using three approaches: the Monte Carlo method (MCM), the Unscented transformation (UT), and the GUM uncertainty framework (GUF). To compare the uncertainty estimations provided by the three methodologies, the irradiance measurement model and the uncertainty sources considered are the same.

### 3.1. Irradiance measurement model

For UV measurements, the equation

$$E^{M}(\lambda) = \frac{S^{M}(\lambda)}{r(\lambda)} \tag{1}$$

is used to derive the solar spectral irradiance $E(\lambda)$ at wavelength $\lambda$. In Eq. (1), $S^{M}(\lambda)$ is the signal measured under the Sun, $r(\lambda)$ is the spectral responsivity of the spectrometer, and $E^{M}(\lambda)$ is the measured UV irradiance.

Therefore, to obtain the spectral irradiance the responsivity of the instrument must be known beforehand. The spectral responsivity is

**Table 1**
Internal temperature, number of dark counts measurements ($N$), mean dark counts, and their associated standard uncertainty measured by Brewer #150 during the calibration campaign.

| Internal temperature (°C) | $N$ | Dark counts (counts per cycle) | Standard deviation of the mean (counts per cycle) |
|---|---|---|---|
| 24 | 15 | 0.1643 | 0.0123 |
| 26 | 13 | 0.2056 | 0.0162 |
| 28 | 15 | 0.3917 | 0.0251 |
| 30 | 23 | 0.5132 | 0.0214 |
| 32 | 35 | 0.8017 | 0.0733 |
| 34 | 39 | 1.2200 | 0.1954 |
| 36 | 38 | 1.6118 | 0.1298 |

determined through the radiometric calibration as

$$r(\lambda) = \frac{S^{L}(\lambda)}{E^{L}(\lambda)}, \tag{2}$$

where $S^{L}(\lambda)$ is the signal recorded under the calibration source, and $E^{L}(\lambda)$ is the spectral irradiance emitted by this source. Brewer spectrometers are frequently calibrated using 1000 W tungsten lamps, with certified irradiance.

Combining Eq. (1) and (2) results in

$$E^{M}(\lambda) = \frac{S^{M}(\lambda) \cdot E^{L}(\lambda)}{S^{L}(\lambda)}. \tag{3}$$

Although the irradiance model described above seems straightforward, the variables involved in the calculation are affected by several sources of uncertainty and must be corrected before the irradiance values can be derived. This results in a complex set of equations and processing algorithms that complicate the uncertainty evaluation.

### 3.2. Uncertainty sources

In this section, the different uncertainty sources and how they affect the spectral UV measurements will be described and characterised. This information is needed for the uncertainty evaluation, independently of the method used for the uncertainty propagation (MCM, UT, or GUF). These uncertainty sources can be divided into three groups, depending on whether they affect (1) the scans measured by the Brewer (noise, dark counts, and dead time of the photomultiplier tube), (2) the instrument responsivity (distance, lamp spectral irradiance, lamp current, and stability), or (3) the unprocessed irradiance (temperature, cosine error, and wavelength misalignment).

In the following, the superscript 'M' will mark the inputs measured outdoors, 'L' will denote those measured during the radiometric calibration, and 'X' will be used to refer to both measurements (X = {M, L}). Furthermore, subscript '0' will denote the raw, uncorrected variables while subscripts '1', '2', etc. will be used to refer to the corrected values of those variables.

#### 3.2.1. Noise

The term noise is used to describe any fluctuation of the measured UV irradiance. In general, it can be classified into two groups: (1) dark noise (see Section 3.2.2) and (b) flux-generated noise. The latter only appears when light reaches the detection system. In UV spectroscopy, it is habitually characterised by repeating the measurement several times and deriving a standard deviation or studying the signal-to-noise ratio SNR (e.g. [25,57,58]). This is straightforward for signals recorded during radiometric calibrations as the emitting source is stable. However, for outdoor measurements the same process is complicated, as noise also depends on solar zenith angle and atmospheric conditions. To overcome this limitation, the methodology set by Bernhard and Seckmeyer [25] was followed. Consequently, the SNR was derived from repeated measurements of the calibration source. Then, the relationship between the SNR and the measured signal was studied and found to be

$$\mathrm{SNR}(\lambda) = 4.22\sqrt{S_0^{X}(\lambda)} \tag{4}$$

Introducing the signal measured under the Sun in Eq. (4) results in a spectral SNR that ranges from 88 % (301 nm and 73.5° SZA) to 0.6 % (360 nm and 32.1° SZA). For the calibration, the SNR depends solely on wavelength and varies between 13 % at 301 nm and 4 % at 360 nm.

#### 3.2.2. Dark counts

Dark counts, also known as dark signal or dark current, is the term habitually used for the counts detected that arise from thermal noise, not UV photons. For Brewer #150, dark counts depend on temperature (the instrument is not temperature-stabilised), but they show no spectral dependency [33].

Brewer MKIII spectrometers automatically determine the dark current by blocking the incoming light and the result is registered in the same file as the UV scan. To correct the signal measured, dark counts must be subtracted from the raw counts registered during the radiometric calibration $S_0^{L}(\lambda)$ and outdoors measurements $S_0^{M}(\lambda)$

$$S_1^{X}(\lambda) = S_0^{X}(\lambda) - D^{X}, \tag{5}$$

where $D^{X}$ are the dark counts registered before each UV scan and $S_1^{X}(\lambda)$ the corrected signal.

To associate an uncertainty to this source, the set of dark counts measurements registered during the campaign was studied. Since dark counts depend on temperature and Brewer #150 has no temperature stabilisation system, dark counts vary throughout the day. To derive an uncertainty, the dark counts measured at each temperature level were averaged and the standard deviation of the mean was calculated from the $N$ available measurements (see Table 1). Table 1 confirms the temperature dependence of Brewer #150 dark counts since their value and standard uncertainty increase as the internal temperature of the instrument rises.

#### 3.2.3. Dead time (non-linearity)

Dead time is the time interval where the detection system is unable to detect a second photon after a first one has been registered. Thus, any photons arriving during this dead time will be recorded as one single count. The probability of missing photons increases with the count rate, i.e. the intensity of the incoming radiation. As a result, the response of Brewer spectroradiometers is non-linear and must be corrected to compensate for the effect of dead time.

For Brewer spectrophotometers, this correction is carried out in an iterative process (index $n$) by assuming Poisson statistics

$$S_2^{X}(\lambda, n+1) = S_1^{X}(\lambda) \cdot \exp\left(\tau S_2^{X}(\lambda, n)\right), \tag{6}$$

where $\tau$ is the dead time, $S_1^{X}(\lambda)$ the corrected signal for dark counts, and $S_2^{X}(\lambda)$ the resulting signal corrected for dead time. As a first approximation in Eq. (6), the true count rate is set to the observed counts, i.e. $S_2^{X}(\lambda, 1) = S_1^{X}(\lambda)$. It is usual to use nine iterations in Eq. (6), although the corrected signal converges after 4–5 iterations [59].

Since Brewer spectrometers measure their dead time daily, a mean and standard deviation can be derived from this continuous monitoring. During the RBCC-E campaign, the dead time of Brewer #150 was $\tau = (26.5 \pm 1.9)$ ns.

#### 3.2.4. Spectral irradiance of reference lamp

As shown in Eq. (2), knowing the spectral irradiance emitted by the reference lamp is essential to determine the responsivity of the instrument. Therefore, the uncertainties of this irradiance must be included in the uncertainty analysis. This is straightforward since Brewers participating in the RBCC-E campaign are calibrated using 1000 W lamps with certified irradiance. As a result, the lamp irradiances and their

associated uncertainties are stated in its calibration certificate. For Brewer #150, the reference lamp was a Optronic Laboratories 1000-Watt Tungsten-Halogen lamp, with serial number 1312. Its expanded spectral uncertainty (coverage factor of k = 2), at 50 cm when operating at 8 A, varies between 1.55 % at 290 nm and 1.21 % at 363 nm.

#### 3.2.5. Electrical current of reference lamp

During the operation of the reference lamp, maintaining the electrical current at the level designated on the calibration certificate is essential. Any deviation from this nominal value will result in different spectral irradiances than those certified [25,60].

Webb et al. [60] found that a 1 % change in the current of the lamp resulted in a 10 % change in its spectral irradiance at 300 nm. Currently, the standard practice is to assume this condition holds for all wavelengths (e.g. [25,27]). However, this ignores the fact that the result of varying the current is more marked at short wavelengths [60]. To include this effect, the methodology set by Schinke et al. [61] has been followed. This consists in simulating the lamp as a black body with spectral irradiance

$$E_{bb}(\lambda, T) \propto \frac{hc}{\lambda^5}\left[\exp\left(\frac{hc}{\lambda k T}\right) - 1\right]^{-1}, \tag{7}$$

where $c$ denotes the speed of light, $h$ the Planck constant, $T$ the operating temperature of the lamp's filament, and $k$ the Boltzmann constant. The filament's temperature $T$ is determined as

$$T = \frac{V + IR_0(\alpha\ T_0 - 1)}{\alpha\ IR_0}, \tag{8}$$

where $R_0$ is the resistance at room temperature $T_0$, $\alpha$ the temperature coefficient of the filament, V the operating voltage, and $I$ the operating current of the lamp. For the reference lamp used in this study, the operating voltage V is 114.2 V, the nominal current $I$ is 8 A, the resistance measured at a room temperature ($T_0 = 300.5$ K) $R_0$ is 0.89 Ω, and the temperature coefficient $\alpha$ is 0.0054 $K^{-1}$ [33]. The operating temperature is thus 3089 K according to Eq. (8).

Therefore, small current changes lead to variations in the temperature of the reference lamp which results in slightly different irradiance values, as shown in Eq. (7)–(8). The setup used during the RBCC-E campaign set the current $I$ at (8.000 ± 0.001) A.

#### 3.2.6. Distance adjustment

To accurately calibrate a spectroradiometer, the distance between the optical reference planes of the diffuser and the emitting lamp must be the one specified in the calibration certificate. Any error committed during the distance adjustment changes the spectral irradiance emitted by the lamp by

$$E_1^L(\lambda) = E_{bb}(\lambda)\left(\frac{d_r}{d_r + \Delta d}\right)^2, \tag{9}$$

where $E_{bb}(\lambda)$ is the spectral irradiance of the reference lamp, $d_r$ the reference distance, $\Delta d$ the deviation from the distance reference, and $E_1^L(\lambda)$ the new values of spectral irradiance. Eq. (9) is valid provided the distance between the lamp and the diffuser is large and the lamp can be regarded as a point source. For 1000 W lamps, the reference distance is 50 cm and Eq. (9) holds.

The uncertainty committed in the distance alignment between the reference lamp and Brewer #150 diffuser has two components. The first one is caused by the instrument used to measure the distance. In the RBCC-E campaign, a ruler with a precision of 0.1 cm was employed. The second component is related to the determination of the reference plane position of the instrument's diffuser. For Brewer #150, the standard uncertainty of this process is 0.015 cm [33]. Combining both components in quadrature results in a standard uncertainty of 0.06 cm.

#### 3.2.7. Radiometric stability

Photomultiplier tubes are one of the preferred detectors to measure solar UV irradiance thanks to their high sensitivity in this wavelength region [62]. However, one of their main drawbacks is their instability. As a result, the sensitivity and, in turn, the responsivity $r(\lambda)$ of the instrument changes with time. This affects the irradiance measured since it is obtained as

$$E_0^M(\lambda) = \frac{S_2^M(\lambda)}{r(\lambda)} = \frac{S_2^M(\lambda)}{S_2^L(\lambda)} E_{bb}(\lambda, T), \tag{10}$$

where $S_2^M(\lambda)$ is the corrected signal measured outdoors, $S_2^L(\lambda)$ the corrected signal measured during the calibration, and $E_{bb}(\lambda, T)$ the irradiance emitted by the reference lamp, as described in Sect. 3.2.5.

To characterise this drift, Bernhard and Seckmeyer [25] suggest studying the difference in responsivity between consecutive calibrations. Applying this methodology to Brewer #150 calibration records resulted in standard uncertainties varying between 3.75 % at 290 nm and 3.24 % at 363 nm.

#### 3.2.8. Temperature correction

Unlike other UV spectroradiometers, Brewer spectrometers have no temperature stabilisation system. As a result, the measured UV irradiance is over or underestimated, depending on the instrument [29,32,63,64].

Although it is well known that their spectral UV measurements are affected by temperature, there is no standard methodology to characterise or correct this temperature dependence. Most studies determine this dependency by placing external lamps on top of the diffuser and performing the measurements while the instrument's temperature increases gradually. For Brewer #150, the dependency was studied outdoors using 100 W and 1000 W lamps [33].

Since the responsivity of Brewer #150 decreases linearly with temperature, its UV irradiance measurements are corrected by applying

$$E_1^M(\lambda) = \frac{E_0^M(\lambda)}{1 + c_T \Delta T}, \tag{11}$$

where $E_0^M(\lambda)$ are the raw values of measured irradiance given by Eq. (10), $c_T$ the temperature correction factor, $E_1^M(\lambda)$ the corrected UV irradiance, and $\Delta T$ denotes the difference between the temperature of the scan and the reference temperature (33 °C). For Brewer #150, the temperature correction factor is $c_T = (-0.0016 \pm 0.0002)\ °C^{-1}$ for the temperature range 23 °C–38 °C [33]. This value was determined by placing two lamps (100 W and 1000 W) on top of the diffuser and measuring the change in the responsivity of Brewer #150 while the temperature of the instrument increased steadily due to Sun heating. This characterization test was carried out on three different days to ensure repeatability. Since the correction factor derived from this procedure showed no spectral dependency [33], the average value $c_T = (-0.0016 \pm 0.0002)\ °C^{-1}$ was chosen as the correction factor for the whole Brewer wavelength range.

#### 3.2.9. Cosine correction

Ideally, the signal recorded by a spectroradiometer should be proportional to the cosine of the angle between the incoming radiation and the normal of the entrance optics. The deviation from this ideal response is known as cosine error. Thus, cosine error is mainly produced by imperfections in the entrance optics and is characteristic of each instrument.

For Brewer MKIII spectroradiometers, cosine error results in the underestimation of the measured UV irradiance and varies typically between 4 % and 15 % [23,29,47,65]. Therefore, to obtain accurate measurements, the cosine error needs to be corrected. Although several methodologies have been developed for correcting this deviation, all of them require the knowledge of (a) the instrument angular response, (b)

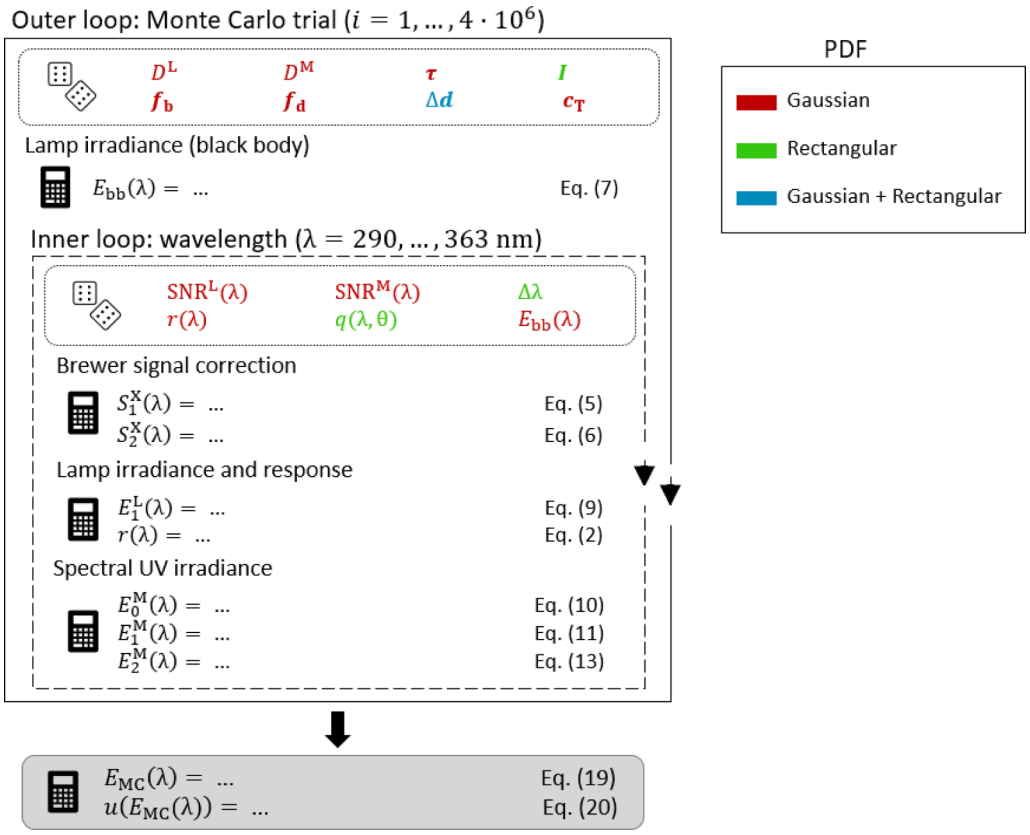



**Fig. 1.** Flow chart for the Monte Carlo simulation adapted from [61]. The dice icons symbolise the sampling of random numbers from three types of probability density functions (PDF): Gaussian (in red), Rectangular (in green), and a combination of Gaussian and rectangular (in blue).

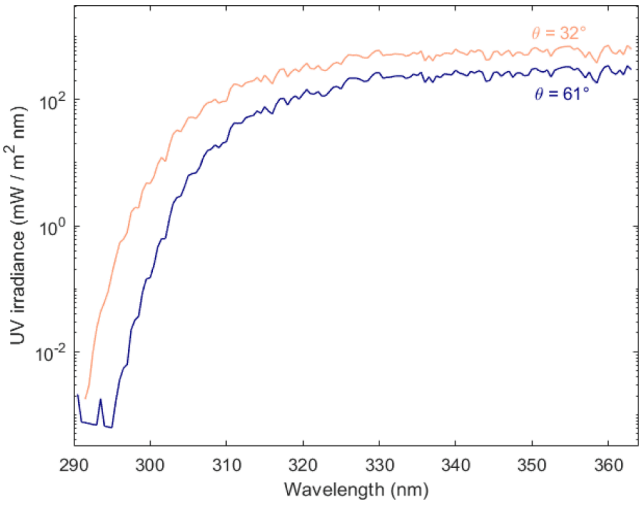



**Fig. 2.** Spectral UV irradiance measured by Brewer #150 on 10 September 2021 (cloudless conditions) at El Arenosillo Observatory in logarithmic scale at two solar zenith angles, 32° and 61°.

the correction factors for the direct and diffuse components of the global irradiance, and (c) the ratio between direct and global irradiance.

In this study, the cosine correction factor at wavelength and solar zenith angle was calculated as [66]

$$R_c(\lambda,\theta) = f_b(\theta)\cdot q(\lambda,\theta) + f_d(1 - q(\lambda,\theta)), \tag{12}$$

where $q(\lambda,\theta)$ is the ratio between direct and global irradiance, $f_b(\theta)$ the correction factor for the direct component, and $f_d$ the correction factor for the diffuse component.

The direct cosine factor $f_b(\theta)$ was determined in the laboratory using the Brewer Angular Test (BAT) and a 150 W Xe lamp with an optic fibre. It varies between 1.002 at 5° and 1.278 at 85°. The standard uncertainty for this factor is 0.003 at 30° incidence angle and 0.007 at 60° incidence angle. The relative standard uncertainty $u(f_b)/f_b$ is 0.3 % at 30° and 0.7 % at 60°. These uncertainty values are caused mainly by misalignment of the BAT and the stability of the Xe lamp.

Regarding the diffuse cosine factor, it was estimated assuming isotropic radiation. This assumption is a reasonable approximation in the UVB region for clear skies [67], but it is generally assumed regardless of the sky conditions (e.g. [47,68,69]). The previous calculation resulted in a factor of $f_d = (0.986 \pm 0.005)$. The standard uncertainty was estimated using the methodology described by Bernhard and Seckmeyer [25] and the data provided by Gröbner et al. [70].

The direct/global ratio was simulated using the libRadtran model [71] under cloud-free and different atmospheric conditions. LibRadtran is a widely used radiative transfer model. It calculates radiances, irradiances, and actinic fluxes in the solar and thermal spectral region for different atmospheric and surface conditions [72]. It has been used for numerous applications such as climate studies, UV forecasting, or the remote sensing of clouds, trace gases, and aerosols in the atmosphere. The libRadtran software package now includes a graphical user interface to simplify its usage [71].

Finally, UV irradiance measurements are corrected for the cosine error by dividing by the correction factor of Eq. (12)

$$E_2^M(\lambda) = \frac{E_1^M(\lambda)}{R_c(\lambda,\theta)} = \frac{S_2^M(\lambda)\cdot E_{bb}(\lambda,T)}{S_2^L(\lambda)\cdot R_c(\lambda,\theta)\cdot(1 + c_T\Delta T)}, \tag{13}$$

where $E_1^M(\lambda)$ is the irradiance corrected for temperature given by Eq. (11).

#### 3.2.10. Wavelength misalignment

The UV intensity changes by more than 5 orders of magnitude (as seen in Fig. 2) between the detection threshold of solar UV radiation, around 290 nm (depending on the elevation of the Sun in the sky, the sensitivity of the instrument, etc.) and around 320 nm. Therefore, small errors committed in the wavelength alignment of a spectrometer cause large deviations in the measured irradiance.

To correct this error source, a wavelength calibration is carried out before field measurements. The wavelength shifts of Brewer spectroradiometers participating in the RBCC-E campaign are obtained using two methodologies. First, the wavelengths measured by the instruments are compared with those corresponding to the emission lines of Hg, Cd, and Zn discharge lamps. Then, the resulting calibration is also checked by comparing the Fraunhofer lines of the measured spectra with the respective ones of a high-resolution reference spectra. This last step is performed using detection algorithms such as SHICRivm [73] or matSHIC [36].

The standard uncertainty of the wavelength calibration has two components. The first one is related to the precision of the system that sets the wavelengths measured by the spectroradiometer. For Brewer spectroradiometers, this system consists of a pair of micrometres and a stepper motor with a precision of approximately 8 pm [74]. The second component is the wavelength shift. As mentioned earlier, this shift can be determined either by using discharge lamps or detection algorithms. However, by using the latter a spectral shift specific for each spectrum measured can be obtained. Therefore, in this work spectral shifts were determined using the SHICrivm software package V. 3.075. For example, the wavelength shift of Brewer #150 UV spectrum recorded on 10 September at a solar zenith angle of 32° (see Fig. 2) varies between 0.03 nm at 300 nm and 0.005 nm at 350 nm.

### 3.3. GUM uncertainty framework

The GUM uncertainty framework (GUF) was implemented following the guidelines set in BIPM et al. [24]. This methodology evaluates the uncertainty of the irradiance (output) by propagating the standard deviations associated with each input of the model, i.e. the error sources (see Sect. 3.2). These standard deviations can be determined by applying type A or type B evaluation procedures [24]. Type A evaluation is used for those input quantities that have been obtained from a series of independent observations, such as dead time or dark counts. In these cases, the arithmetic mean of the repeated observations is taken as the best estimate and the standard deviation of the mean as the standard uncertainty. On the other hand, type B evaluation assigns a standard deviation based on a priori distributions and general knowledge. This is the case for those inputs that may depend on manufacturer's specifications, previous measured data, calibration certificates, etc. For example, the standard uncertainties of the current and spectral irradiance of the reference lamp are type B uncertainties.

Once a standard deviation has been assigned to each uncertainty source, the combined standard uncertainties of spectral UV measurements are obtained by applying the law of propagation of uncertainties (LPU) to Eq. (13). This results in the following

$$\frac{u\left(E_2^{\mathrm{M}}(\lambda)\right)}{E_2^{\mathrm{M}}(\lambda)}=\sqrt{\left[\frac{u\left(S_2^{\mathrm{M}}(\lambda)\right)}{S_2^{\mathrm{M}}(\lambda)}\right]^2+\left[\frac{u\left(S_2^{\mathrm{L}}(\lambda)\right)}{S_2^{\mathrm{L}}(\lambda)}\right]^2+\left[\frac{u(E_{\mathrm{bb}}(\lambda,T))}{E_{\mathrm{bb}}(\lambda,T)}\right]^2+\left[\frac{u(c_{\mathrm{T}})\Delta\mathrm{T}}{1+\mathrm{c_T}\Delta\mathrm{T}}\right]^2+\left[\frac{u(R_{\mathrm{c}}(\lambda,\theta))}{R_{\mathrm{c}}(\lambda,\theta)}\right]^2}, \tag{14}$$

where $S_2^{\mathrm{L}}(\lambda)$ is the dead-time corrected signal measured during the calibration, $S_2^{\mathrm{M}}(\lambda)$ the dead-time corrected signal measured outdoors, $E_{\mathrm{bb}}(\lambda,T)$ the spectral irradiance emitted by the reference lamp, $c_{\mathrm{T}}$ the temperature coefficient, $R_{\mathrm{c}}(\lambda,\theta)$ the spectral cosine correction factor, and $E_2^{\mathrm{M}}(\lambda)$ the measured spectral UV irradiance after correcting for temperature and cosine error effects. Their corresponding standard uncertainties are indicated by letter $u$.

Note that Eq. (14) is only valid for linear models and uncorrelated uncertainty sources. To account for the non-linearity of the irradiance model, higher-order terms in the Taylor series expansion should have been included in the uncertainty evaluation (see [24]). However, since this is highly complicated for spectral UV measurements, the non-linearity of the model has been disregarded. Furthermore, if the uncertainty sources are correlated a covariance term must also be added in Eq. (14), as indicated by [24]. Since the uncertainty sources considered in this study are uncorrelated, Eq. (14) holds.

Some of the uncertainties involved in Eq. (14) have already been determined, such as the uncertainty of the temperature coefficient (see Sect. 3.2.8). The rest must be calculated by further deriving.

The uncertainties associated with the signals, measured outdoors and during the calibration, are obtained by deriving Eq. (6)

$$u^2\left(S_2^{\mathrm{X}}(\lambda)\right)=\frac{\exp\left(2\tau S_2^{\mathrm{X}}(\lambda)\right)\cdot u\left(S_1^{\mathrm{X}}(\lambda)\right)+u^2(\tau)\left(S_2^{\mathrm{X}}(\lambda)\right)^4}{1-\left(\tau S_2^{\mathrm{X}}(\lambda)\right)^2}, \tag{15}$$

where $u(\tau)$ is the uncertainty of the dead time (1.9 ns as determined in Sect. 3.2.3) and $u\left(S_1^{\mathrm{X}}(\lambda)\right)$ is the uncertainty of $S_1^{\mathrm{X}}(\lambda)$ at wavelength $\lambda$. Since this signal is affected by dark count correction and noise, its spectral uncertainty is calculated by deriving Eq. (5) and using the definition of the signal-to-noise ratio

$$u^2\left(S_1^{\mathrm{X}}(\lambda)\right)=\left(\frac{S_0^{\mathrm{X}}(\lambda)}{\mathrm{SNR}(\lambda)}\right)^2+u^2\left(D^{\mathrm{X}}\right), \tag{16}$$

where $u\left(D^{\mathrm{X}}\right)$ is the standard uncertainty of the dark counts measured (see Table 1) and $\mathrm{SNR}(\lambda)$ is the spectral signal-to-noise ratio (their values are described in Sect. 3.2.1).

Regarding the cosine correction factor, its uncertainty is determined by deriving Eq. (12)

$$u^2(R_{\mathrm{c}}(\lambda,\theta))=u^2(f_{\mathrm{b}}(\theta))[f_{\mathrm{b}}(\theta)-f_{\mathrm{d}}]^2+u^2(q(\lambda,\theta))f_{\mathrm{b}}^2(\theta)+u^2(f_{\mathrm{d}})[1-q(\lambda,\theta)]^2, \tag{17}$$

where $q(\lambda,\theta)$ is the ratio between direct and global irradiance, $f_{\mathrm{b}}(\theta)$, and $f_{\mathrm{d}}$ denote the correction factors for the direct and the diffuse component, respectively. Their values and corresponding uncertainties were determined in Sect. 3.2.9.

Finally, the uncertainties of the irradiance lamp $E_{\mathrm{bb}}(\lambda,T)$ are calculated using Eq. (7), (8), and (9)

$$\frac{u^2(E_{\mathrm{bb}}(\lambda,T))}{E_{\mathrm{bb}}(\lambda,T)}=\left[\frac{u_{\mathrm{c}}(\lambda)}{2E_{\mathrm{bb}}(\lambda,T)}\right]^2+\frac{(d_{\mathrm{r}}+u(\Delta\mathrm{d}))^2-d_{\mathrm{r}}^2}{d_{\mathrm{r}}^2}+\left\{\frac{hc\cdot V\cdot u(I)}{\alpha k I^2\lambda^6T^3}\left[1+\left(\exp\left(\frac{hc}{\lambda kT}\right)-1\right)^{-1}\right]\right\}^2, \tag{18}$$

where $u(\Delta\mathrm{d})$ is the uncertainty committed in the distance adjustment (0.06 cm), $u_{\mathrm{c}}(\lambda)$ the expanded uncertainties stated in the calibration certificate (see Sect. 3.2.4), and $u(I)$ denotes the uncertainty of the lamp's current (1 mA).

Furthermore, it should be noted that wavelength shift and

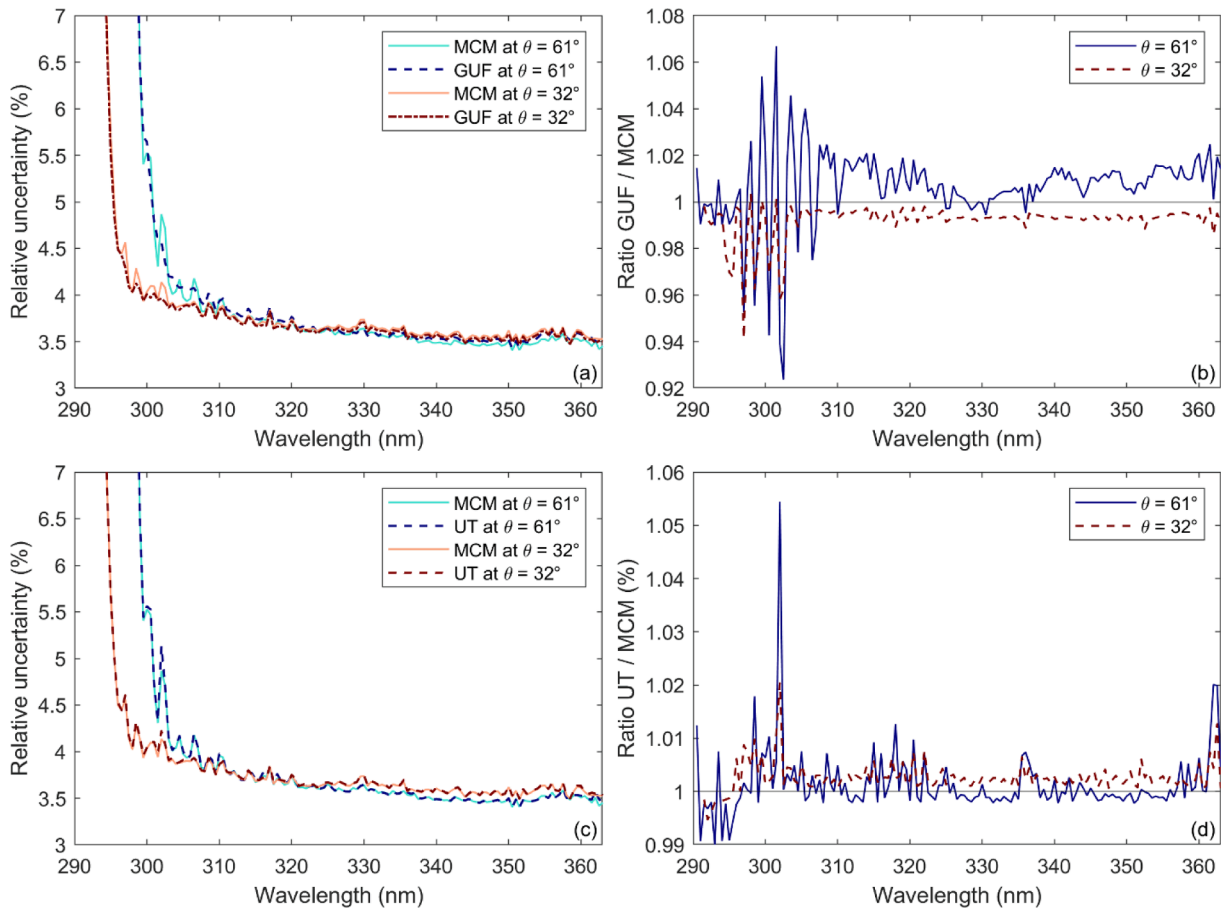



**Fig. 3.** Comparison of the MCM, UT, and GUF methodologies for the estimation of the uncertainty of the global UV irradiances shown in Fig. 2. (a) Relative combined standard uncertainties provided by the MCM and GUF methods at 61° and 32° SZAs. (b) Spectral ratio between the uncertainty estimated by the GUF and the MCM at 61° and 32°. (c) Relative combined standard uncertainties estimated by the MCM and UT techniques at 61° and 32° SZAs. (d) Spectral ratio between uncertainties estimated by the UT and the MCM at 61° and 32°.

radiometric stability are not included in Eq. (14). As mentioned in Sect. 3.2.10 wavelength misalignment is corrected by using additional software (SHICRivm) and as a result, is complicated to obtain its partial derivative. To include this source in the analysis, the methodology proposed by Bernhard and Seckmeyer [12] has been followed. This consists in comparing the UV spectrum recorded by the instrument (a) with its wavelength error and (b) with no wavelength shifts. To obtain this ratio, the UV irradiance must be simulated using a radiative transfer model and then convolved with the slit function of the spectroradiometer. In this work, the libRadtran model has been used. Once the ratio was calculated it was combined in quadrature with the other uncertainty components of Eq. (14). Regarding the instability, its uncertainty is easily obtained by studying the responsivity drift. The resulting relative spectral uncertainty (3.75 % at 290 nm) was also added in quadrature in Eq. (14).

Finally, the contribution of each error source to the combined standard uncertainty is obtained by studying the sensitivity coefficients, i.e. the partial derivative of the UV irradiance with respect to the different uncertainty sources. This is straightforward since these quantities have already been determined for the uncertainty evaluation and are shown in Eq. (14).

### 3.4. Monte Carlo method

The Monte Carlo method (MCM) is a numerical approach for the evaluation of measurement uncertainty. It is valid for any model that provides a single and well-defined output quantity, as is the case for spectral UV irradiance. The uncertainty evaluation is carried out by calculating a large number of times (N) the output quantity (the measured UV irradiance) while varying the uncertainty sources according to their probability density function (PDF). Then, from all the generated values $E_{G,1}(\lambda), \cdots, E_{G,N}(\lambda)$ an estimate and the associated combined standard uncertainty can be derived

$$E_{MC}(\lambda) = \frac{1}{N}\sum_{j=1}^{N} E_{G,j}(\lambda), \tag{19}$$

$$u(E_{MC}(\lambda)) = \sqrt{\frac{1}{N-1}\sum_{j=1}^{N}\left(E_{G,j}(\lambda) - E_{MC}(\lambda)\right)^2}. \tag{20}$$

The Monte Carlo simulation was implemented following the methodology set in González et al. [37]. Therefore, the number of Monte Carlo trials, $N = 4{\cdot}10^6$, was determined using an adaptive Monte Carlo method, as described in the Supplement 1 to the GUM [14]. This consists in defining a numerical tolerance based on the number of significant decimal digits associated with the standard uncertainty. Then, M Monte Carlo trials are carried out to derive the irradiance and its standard deviation. If the standard deviation exceeds the numerical tolerance previously defined, another M trials are carried out and the standard deviation is recalculated using the 2M irradiance values simulated. This process continues indefinitely by increasing the Monte Carlo iterations until the standard deviation is smaller than the tolerance. To ensure two significant decimals in the combined standard uncertainty of the Brewer UV irradiance, $4{\cdot}10^6$ trials are needed. On the other hand, two types of PDFs have been considered for the uncertainty sources: gaussian and

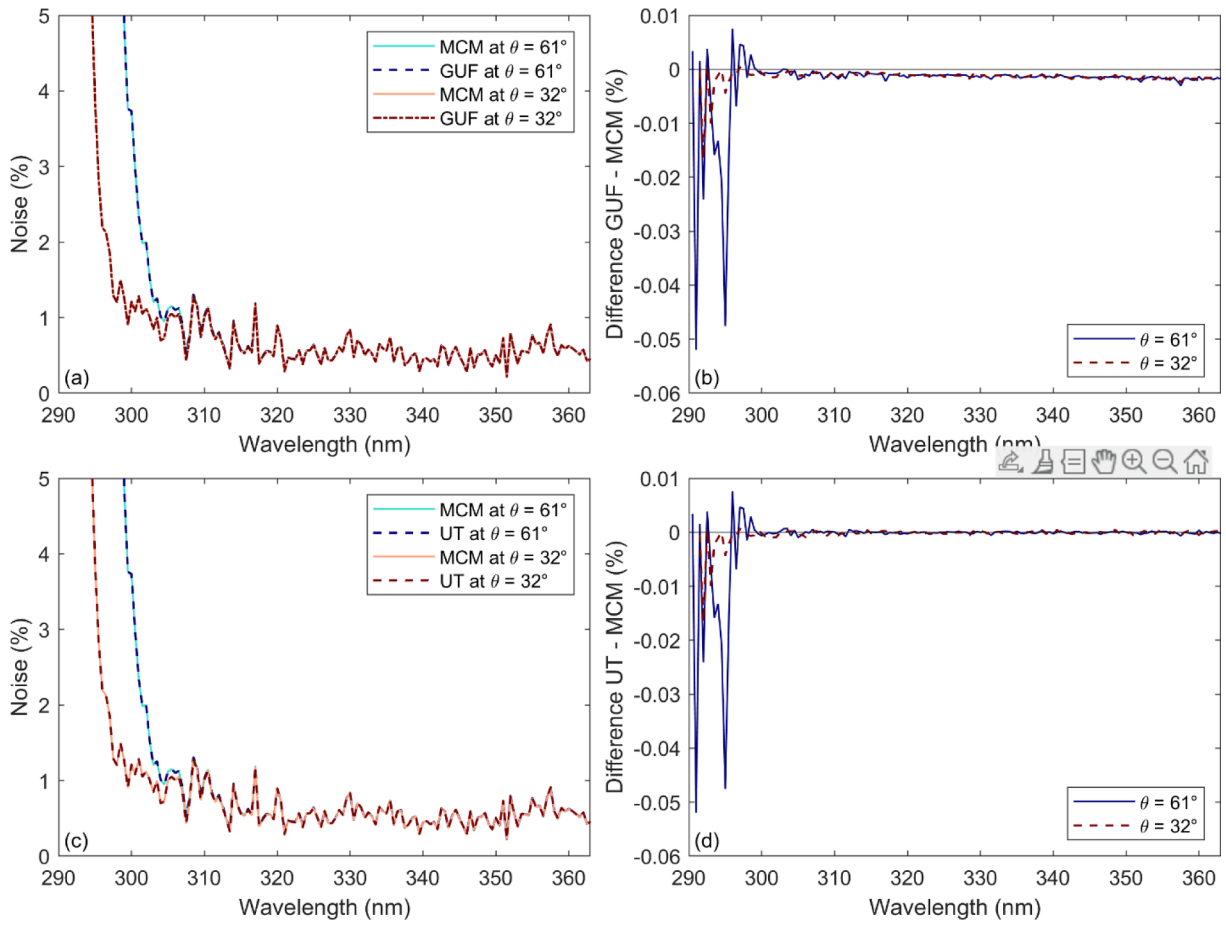



**Fig. 4.** Comparison of MCM, UT, and GUF estimations of the uncertainty caused by noise at two SZAs, 32° and 61°. (a) Relative spectral uncertainty produced by flux-generated noise as estimated by the MCM and the GUF. (b) Absolute difference between the relative uncertainties estimated by the GUF and the MCM. (c) Relative spectral uncertainty caused by noise as estimated by the UT and the MCM. (d) Absolute difference between the relative uncertainties provided by the UT and the MCM.

rectangular. As recommended by the GUM, the rectangular PDF is assigned to those variables that lie in a fixed interval of values without a preferred one. For example, the current of the lamp lies within 7.999 and 8.001 A and any value within this range is equally possible. In this case, the rectangular PDF is the most appropriate. On the other hand, the gaussian PDF is used for those variables that have a best estimate and an associated uncertainty that declines as one departs from this best estimate, i.e. the more probable value. As shown in Fig. 1, the Monte Carlo evaluation has two loops: one for the number of trials and another one for the wavelengths. This is necessary as certain uncertainty sources depend on the wavelength, such as the cosine correction or the spectral irradiance of the reference lamp.

Besides the combined standard uncertainty, the MCM also allows for the calculation of the sensitivity coefficients, i.e. the influence of each source to the total uncertainty budget. This is carried out by running the uncertainty evaluation while holding all uncertainty sources but one fixed at their best estimates [14]. This practice is useful to reduce the uncertainty of the measurement, as it identifies the dominant uncertainty sources.

### 3.5. Unscented transformation

The Unscented transformation (UT) is a numerical method for the uncertainty evaluation that does not require the calculation of the sensitivity coefficients (described in Sect. 3.3). It is based on the principle that the PDF of a n-dimensional set of input quantities (the uncertainty sources) can be approximated using a minimal set of carefully chosen points, the so-called sigma points. These points are defined so that their statistics match the true mean and covariance of the input variables. Then, each sigma point is propagated through the non-linear system (the irradiance model), leading to a cloud of output values. From this set of generated values, an estimate for the mean and covariance of the output can be derived. Despite the similarities between the UT and the MCM, the main difference is that the UT is based on a deterministic approach instead of the random sampling used in the MCM. As a result, the number of sigma points needed is small and the computational cost of implementing the UT is comparable to the one of the GUF.

In the following, the steps necessary to implement the UT are described. The methodology followed is similar to the one used in other studies (e.g. [40,75]). Let us consider propagating the input variable $\boldsymbol{x}$ with dimension n through the non-linear irradiance model. Assuming $\boldsymbol{x}$ has mean $\overline{\boldsymbol{x}}$ and covariance $\boldsymbol{P}_{\mathrm{x}}$, 2n + 1 sigma points $\chi_i$ are formed according to the following

$$\begin{aligned}
\chi_0 &= \overline{\boldsymbol{x}} \\
\chi_1 &= \overline{\boldsymbol{x}} + \left(\sqrt{(\mathrm{n}+\lambda_{\mathrm{U}})\boldsymbol{P}_{\mathrm{x}}}\right)_i,\ i = 1, \cdots, \mathrm{n} \\
\chi_1 &= \overline{\boldsymbol{x}} - \left(\sqrt{(\mathrm{n}+\lambda_{\mathrm{U}})\boldsymbol{P}_{\mathrm{x}}}\right)_i,\ i = \mathrm{n}+1, \cdots, 2\mathrm{n}
\end{aligned} \tag{21}$$

where $\left(\sqrt{(n+\lambda_{\mathrm{U}})\boldsymbol{P}_{\mathrm{x}}}\right)_i$ is the $i$th row of a matrix square root and $\lambda_{\mathrm{U}}$ is a scaling factor, defined as $\lambda_{\mathrm{U}} = \alpha^2(\mathrm{n}+\kappa) - \mathrm{n}$ with $\alpha \in (0, 1]$ and $\kappa \geq 0$. The parameters $\alpha$ and $\kappa$ define how far away the sigma points are from

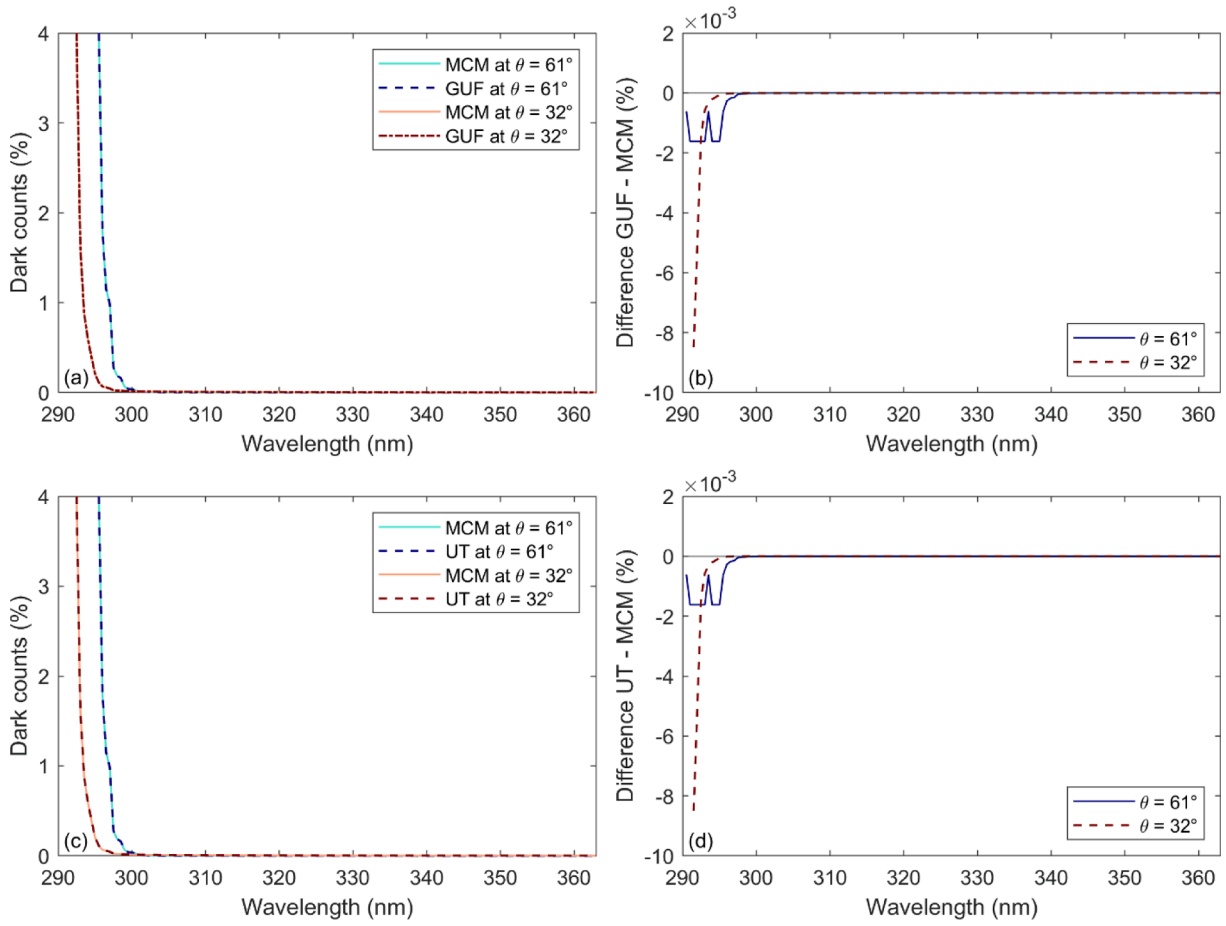



**Fig. 5.** Comparison of MCM, UT, and GUF estimations of the uncertainty arising from dark counts at two SZAs, 32° and 61°. (a) GUF and MCM estimations of the relative spectral uncertainty produced by dark counts. (b) Absolute difference between the relative uncertainties estimated by the GUF and the MCM. (c) Relative spectral uncertainty caused by dark counts as estimated by the UT and MCM. (d) Absolute difference between the UT and MCM estimations of dark counts contribution.

the mean. The scaling factor is usually referred to as λ in the literature, however, to avoid confusion with the wavelength measured by the Brewer, it is denoted as $\lambda_U$.

Once the sigma points are defined, they are propagated through the non-linear irradiance model, generating a new set of irradiance values $E_{G,0}(\lambda), \cdots, E_{G,2n}(\lambda)$. From these generated values, the estimate and its associated uncertainty are calculated as follows

$$E_{UT}(\lambda) = \sum_{i=0}^{2n} W_i^m E_{G,i}(\lambda) \tag{22}$$

$$u(E_{UT}(\lambda)) = \sum_{i=0}^{2n} W_i^c \left(E_{G,i}(\lambda) - E_{UT}(\lambda)\right)\left(E_{G,i}(\lambda) - E_{UT}(\lambda)\right)^T \tag{23}$$

where $W_i^m$ and $W_i^c$ are the weights associated with the sigma points. They are given by

$$W_0^m = \lambda_U/(n+\lambda_U)$$

$$W_0^c = W_0^m + (1-\alpha^2+\beta)$$

$$W_i^m = W_i^c = 1/[2(n+\lambda_U)],\ i = 1, \cdots, 2n \tag{24}$$

For Gaussian input variables, $\beta = 2$ is optimal [38]. For non-Gaussian input variables, Turner and Rasmusen [76] recommend setting $\beta = 0$.

Regarding the sensitivity analysis (the contribution of each uncertainty source to the combined standard uncertainty), it was carried out by forming the sigma points for each uncertainty source while holding all the remaining sources fixed at their best estimate.

## 4. Results

Although the uncertainty evaluation was performed for all cloud-free scans measured, the results obtained were very similar in all cases. Therefore, only the results corresponding to 10 September 2021 are shown in this section. This day was selected as it presents the minimum solar zenith angle (32°) of the campaign and cloudless sky conditions.

Fig. 2 shows the spectral UV irradiance measured by Brewer #150, the physical quantity whose uncertainty will be studied throughout this section. Due to ozone absorption, the measured UV irradiance decreases considerably in the UVB region (from 280 to 315 nm). For example, at 32°, it increases from 0 mW m$^{-2}$ nm$^{-1}$ at 290 nm to 331 mW m$^{-2}$ nm$^{-1}$ at 320 nm. For longer wavelengths, the solar UV spectrum almost levels off. Furthermore, the recorded irradiance also depends on the solar zenith angle (SZA), increasing as SZA declines. In fact, the values measured at a SZA of 32° doubles the ones recorded at 61° SZA for wavelengths above 320 nm.

The combined standard uncertainty determined by the three methods (MCM, UT, and GUF) is presented in Sect. 4.1. Furthermore, the uncertainties arising from each error source were also estimated using all methodologies and the results are compared in Sect. 4.2.

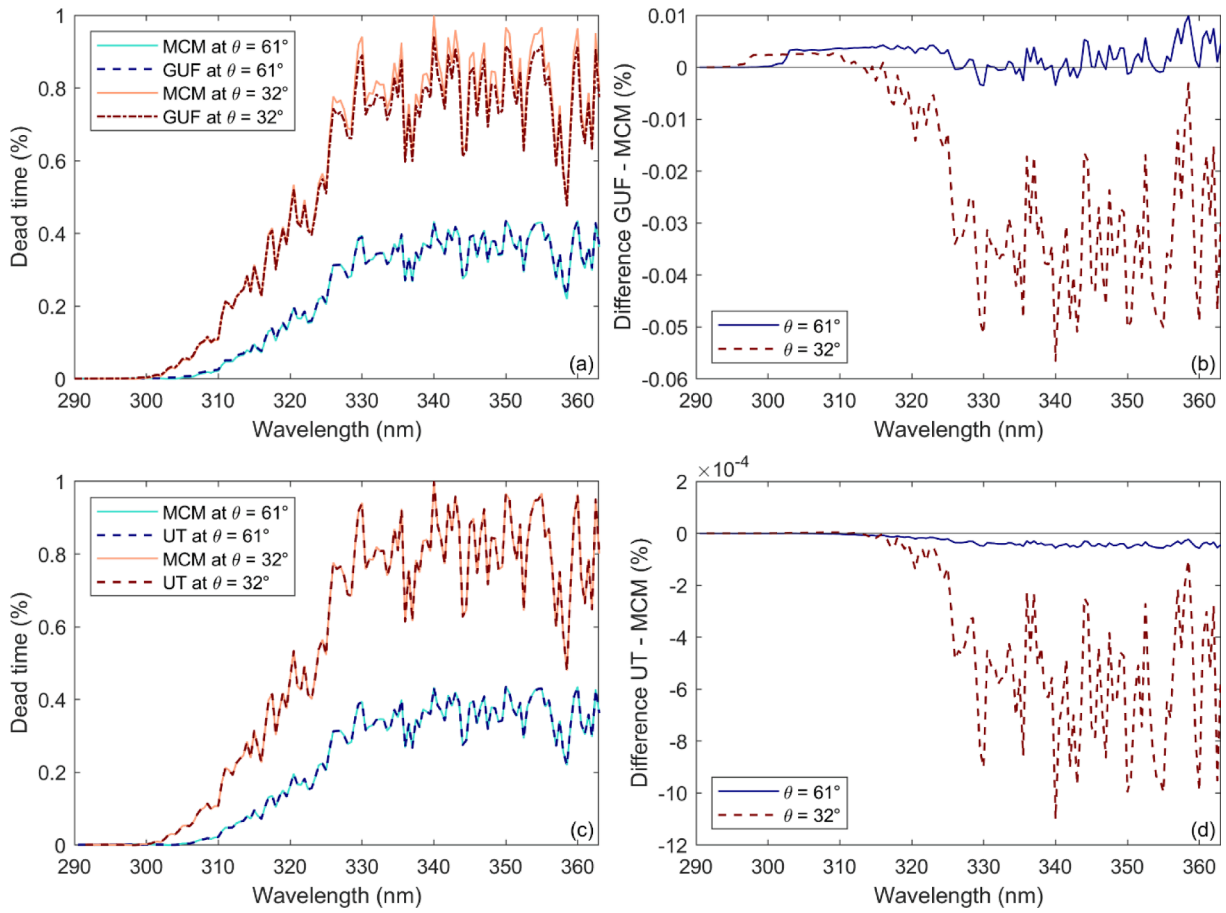



**Fig. 6.** Comparison of MCM, UT, and GUF estimations of the uncertainty produced by the PMT dead time at two SZAs, 32° and 61°. (a) GUF and MCM relative spectral uncertainty caused by dead time. (b) Absolute difference between the relative uncertainties estimated by the GUF and the MCM. (c) UT and MCM relative spectral uncertainties produced by dead time. (d) Absolute difference between the relative uncertainties estimated by the UT and the MCM.

### 4.1. Combined standard uncertainty

To assess the reliability of the GUM uncertainty framework (GUF) and the Unscented Transformation (UT), the combined standard uncertainties estimated by these methodologies will be compared to those of the Monte Carlo method (MCM). The data used are the spectral UV measurements recorded on 10 September 2021 (see Fig. 2). The relative combined standard uncertainties of Brewer #150 UV irradiance for the wavelength range 290–363 nm as estimated by the three methods (GUF, UT, and MCM) are shown in Fig. 3.

Fig. 3a and 3c show that the relative combined standard uncertainty decreases as wavelength increases. For wavelengths below 300 nm, the relative uncertainty, $u\left(E_2^{\mathrm{M}}(\lambda)\right)/E_2^{\mathrm{M}}(\lambda)$, increases abruptly since the irradiance comes close to zero as wavelength approaches 290 nm (see Fig. 2). Furthermore, at short wavelengths, below 310 nm, it depends considerably on the solar zenith angle (SZA), increasing with SZA. For example, at 300 nm, the relative uncertainty (provided by the MCM) is 5.5 % at 61° SZA and 4.0 % at 32° SZA. Furthermore, it is evident from Fig. 3a and 3c that the uncertainties obtained with the GUF and UT approaches follow with very good agreement those of the MCM. It should be noted that the MCM and UT estimations are noisier than those provided by the GUF. These spikes are mainly produced by wavelength misalignment and can be observed in other Monte Carlo simulations [33,57,61,77].

To validate the GUF and UT methodologies, the spectral ratios between the uncertainty estimations provided by these techniques and the MCM is analysed. It can be seen from Fig. 3b that the spectral ratio GUF/MCM decreases with SZA. For the wavelength range 310–360 nm, its average value is 1.008 at 61° SZA and 0.994 at 32° SZA. Moreover, for this wavelength region the ratio is very stable, to within 3 %. At shorter wavelengths, below 310 nm, the ratio fluctuates rapidly, especially at large SZAs. This is produced due to the larger spikes estimated by the MCM in this wavelength region (see Fig. 3a). On the other hand, for these wavelengths the ratio between the GUF and the MCM increases. This is also caused by wavelength misalignment. Between 300 and 310 nm, as SZA increases, wavelength shift becomes one of the dominant uncertainty sources (see Sect. 4.2.11). Since this is one of the uncertainty sources with the larger discrepancies between the GUF and the MCM (see Sect. 4.2.10), the difference in the combined standard uncertainty and, in turn, the ratio between the two methods increases. Regarding the UT/MCM ratio, it also fluctuates due to wavelength misalignment, especially at 302 nm, where the UT overestimates the spike. It depends on the SZA, increasing slightly as SZA decreases and is stable to within 2 %. For the wavelength range 310–360 nm, the average ratio is 1.001 at 61° SZA and 1.003 at 32° SZA. Therefore, for this wavelength region, the UT provide more accurate estimations than the GUF as the UT/MCM ratio is more stable (to within 2 %) and closer to unity than the GUF/MCM. Nevertheless, the agreement between the two methodologies and the MCM is satisfactory as the spectral ratios are close to unity and vary within less than 7 % for the GUF and 6 % for the UT, regardless of SZA and wavelength.

### 4.2. Influence of the uncertainty sources

In this section, the uncertainty arising from each error source individually will be analysed. This sensitivity study is instructive to analyse

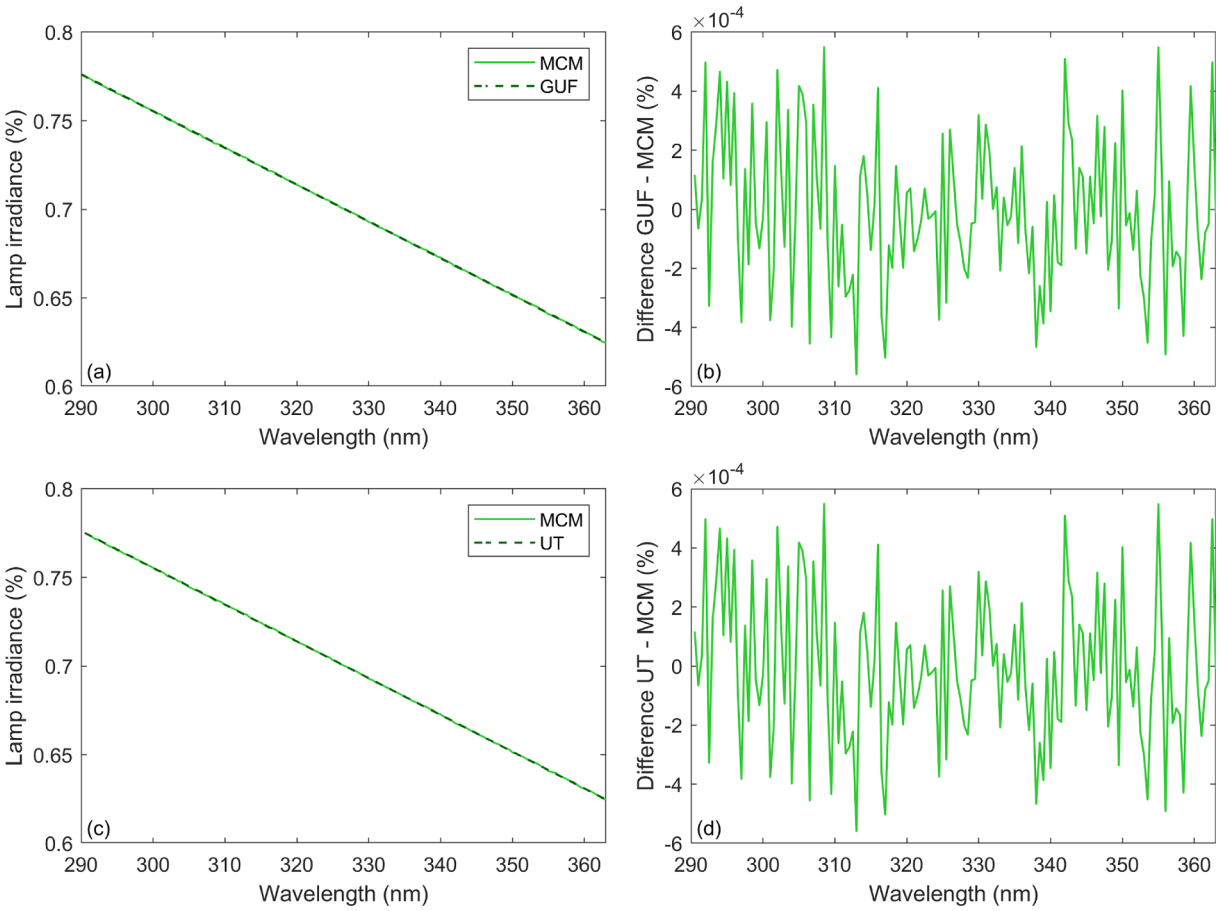



**Fig. 7.** Comparison of MCM, UT, and GUF estimations of the uncertainty produced by the spectral irradiance of the reference lamp. (a) GUF and MCM relative spectral uncertainties caused by the lamp irradiance. (b) Absolute difference between the relative uncertainties estimated by the GUF and the MCM. (c) UT and MCM relative spectral uncertainties produced by the lamp irradiance. (d) Absolute difference between the relative uncertainties estimated by the UT and the MCM.

the influence of each uncertainty source on Brewer UV measurements. Furthermore, it can also be used to check if the GUF and UT approaches correctly estimate every uncertainty contribution. Therefore, for the uncertainty sources described in Sect. 3.2, the absolute difference between the results of the two methodologies (GUF or UT) and those of the MCM will be studied. The ratio or the relative difference between the methods are not suitable to perform this validation. The contribution of certain uncertainty sources (noise, dark counts, or dead time) come close to 0 as wavelength decreases. As a result, the ratio and the relative difference increase dramatically which might mislead the validation.

It should be noted that the units of the absolute difference between the two approaches will be in % since the quantities being compared are relative uncertainties, expressed in %.

#### 4.2.1. Noise

As shown in Fig. 4a and 4c, the uncertainty arising from the signal's noise depends on SZA and wavelength. For 61° SZA, the noise contribution decreases from 3.7 % at 300 nm to 0.6 % at 360 nm. For 32° SZA, it varies between 1.2 % at 300 nm and 0.6 % at 360 nm. Thus, at large wavelengths, beyond 300 nm, the uncertainty produced by noise is independent of solar zenith angle. Therefore, as wavelength rises and SZA declines the UV irradiance measured increases (see Fig. 2) and as a result, the influence of noise decreases.

The GUF, UT, and MCM methodologies overlap in Fig. 4a and 4c, independently of the SZA. In fact, the average absolute difference between the GUF and the MCM is −0.0.0023 % at 61° and −0.0014 % at 32°. For the UT, the corresponding average absolute difference from the MCM is smaller of −0.0012 % at 61° SZA and −0.00035 % at 32°. The difference between the two methodologies and the MCM increase at short wavelengths and high SZAs. These differences are computational and could be further reduced by increasing the number of Monte Carlo trials. However, this results in high computation times and the current differences are small, less than 0.06 % for all wavelengths and SZA measured (see Fig. 4b and 4d). Therefore, the GUF and UT accurately estimate the noise contribution. This was expected since the partial derivation for this uncertainty source is straightforward and a gaussian distribution accurately describes the behaviour of the flux-generated noise.

#### 4.2.2. Dark counts

Fig. 5a and 5c provide information about the relative uncertainty produced by dark counts. It is almost independent of wavelength and SZA for wavelengths above 300 nm. For this wavelength region, dark counts contribution levels off at around 0.002 %. Consequently, the influence of dark counts can be considered negligible in the UVA region. As a result, this error source is usually overlooked in uncertainty evaluation studies (e.g. [31,34]).

The estimations obtained by the two approaches are in very good agreement with the MCM, overlapping in Fig. 5a and 5c. To quantify the discrepancies between the GUF and the UT with the MCM, the absolute difference can be studied. For wavelengths larger than 300 nm, the GUF-MCM difference is less than 1E-6 % independently of the SZA measured. At shorter wavelengths, the difference increases modestly, to within 0.008 %. Regarding the UT, its difference is less than 1E-7 % for the 300–360 nm region, regardless of the SZA measured. Similarly to the GUF, its difference with the MCM increases for short wavelengths

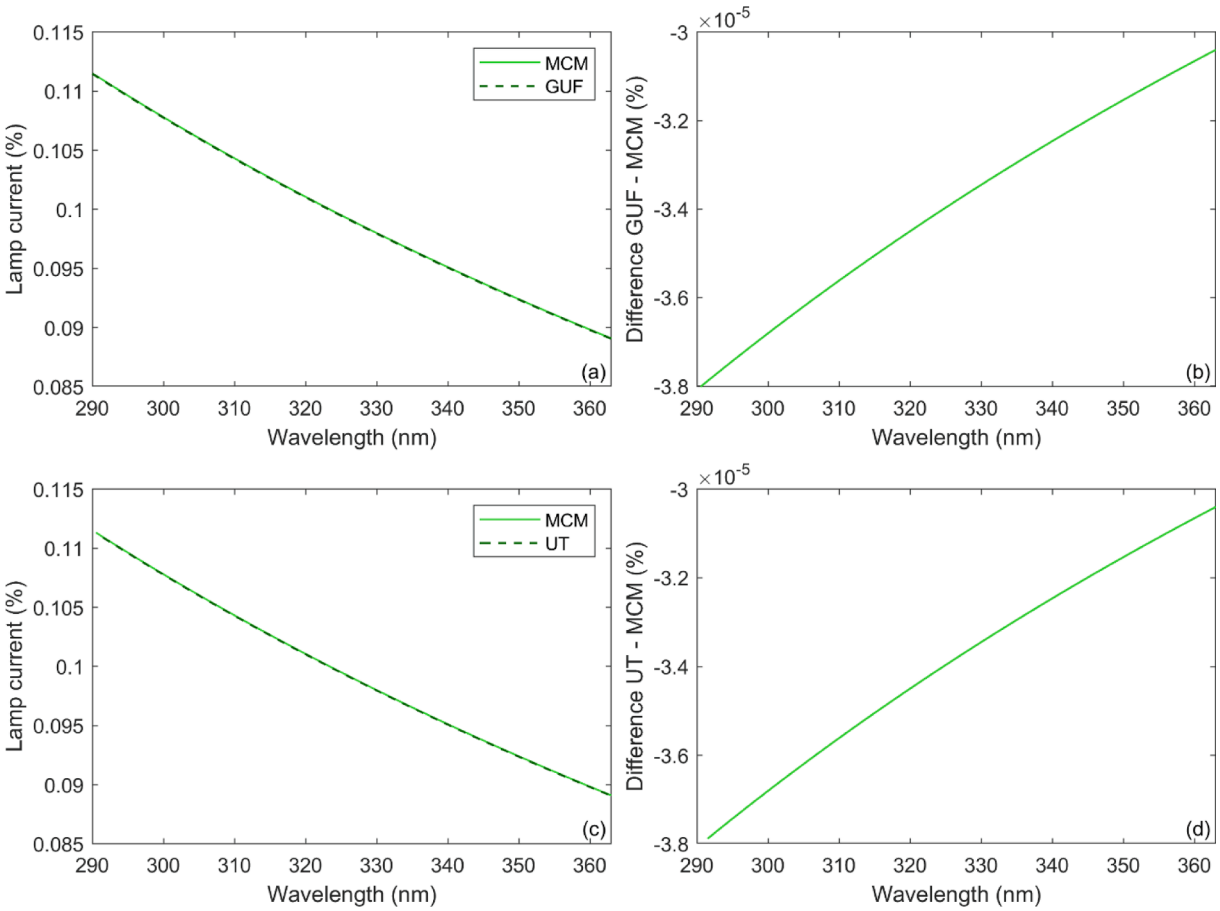



**Fig. 8.** Comparison of MCM, UT, and GUF estimations of the uncertainty produced by the current of the reference lamp. (a) GUF and MCM relative spectral uncertainties caused by the lamp current. (b) Absolute difference between the relative uncertainties estimated by the GUF and the MCM. (c) UT and MCM relative spectral uncertainties produced by the lamp current. (d) Absolute difference between the UT and the MCM for the relative uncertainties.

(below 300 nm) and low SZAs up to 0.008 %. Therefore, the GUF and UT methodologies provide highly consistent values of the dark counts' contribution.

#### 4.2.3. *Dead time (non-linearity)*

The uncertainty arising from dead time increases as wavelength grows and SZA decreases (see Fig. 6a and 6c). In fact, for 61° SZA, the dead time contribution (estimated by the MCM) rises to 0.44 % while for 32° SZA it levels off at around 0.81 %. This behaviour was expected since the effect of dead time of the photomultiplier tube (PMT) increases with the intensity of the radiation reaching the detector system. This happens precisely as wavelength increases and SZA decreases, as shown in Fig. 2.

It can be seen from Fig. 6b that the GUF approach slightly underestimates the dead time contribution as the SZA declines. The absolute difference between the two methods is, on average, 0.002 % and −0.02 % at 61° and 32° SZA, respectively. This slight increase with SZA is likely caused by the mathematical differences in the GUF and the MCM calculations. This translates in relative differences, for the 330–360 nm region, of 0.74 % at 61° SZA and 4.1 % at 32°. Therefore, the agreement between the two methods is satisfactory.

Fig. 6c show the UT and the MCM estimations overlap. In fact, the difference between the two methodologies (see Fig. 6d) is less than 0.001 %. On average, the absolute difference UT-MCM also increases with declining SZA, from −4.5E-5 % at 61° to −2.4E-4 % at 32°. Furthermore, the UT estimations are more precise than those of the GUF, with relative differences from the MCM of 0.02 % at 61° and 0.05 % at 32° between 330 and 360 nm.

#### 4.2.4. *Spectral irradiance of reference lamp*

Fig. 7a and 7c show that the relative uncertainties arising from the lamp irradiance decrease gradually with wavelength, from 0.78 % at 290 nm to 0.62 % at 363 nm. Additionally, this error source has no angular dependency as it affects the responsivity of the instrument. As a result, it has the same influence on all UV measurements as indicated by Eq. (1). All uncertainty sources produced during the radiometric calibration (i.e. distance, current of the reference lamp, and radiometric stability) will also show no SZA dependency.

Regarding the validation, the absolute difference between the relative uncertainties provided by the GUF, the UT, and those of the MCM are virtually zero and shows no significant spectral dependency. Their differences are, on average, −6.61E-6 % for both the GUF-MCM and the UT-MCM. Moreover, these differences fluctuate between 6E-4 % (see Fig. 7b and 7d). Consequently, the GUF and UT estimate precisely this uncertainty contribution.

#### 4.2.5. *Current of reference lamp*

The spectral uncertainty produced by the electrical current of the reference lamp decreases gradually from 0.11 % at 300 nm to 0.09 % at 363 nm (see Fig. 8a and 8c). Therefore, the methodology used to estimate the influence of the electrical current on UV measurements reproduces the fact that this effect is more marked at short wavelengths. However, it slightly underestimates the uncertainties according to the standard methodology. As mentioned in Sect. 3.2.6, the standard methodology assumes that a 1 % change in the electrical current results in a 10 % change in the lamp output. According to this rule, since the error of the lamp electrical current is 0.0125 %, the expected change in

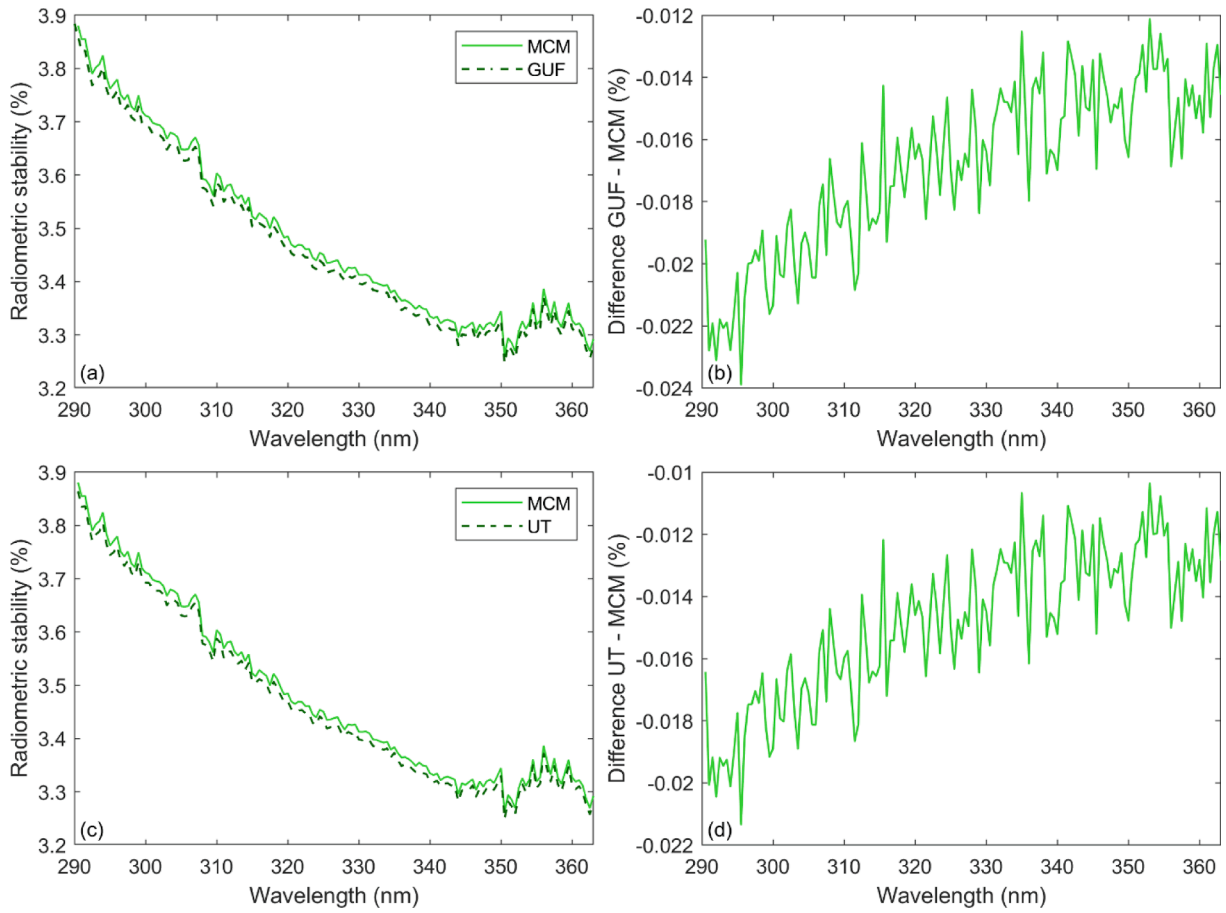



**Fig. 9.** Comparison of MCM, UT, and GUF estimations of the uncertainty produced by the radiometric stability of Brewer #150. (a) Relative spectral uncertainty caused by the instability as estimated by the GUF and the MCM. (b) Absolute difference between the relative uncertainties estimated by the GUF and the MCM. (c) Relative spectral uncertainty produced by the instability as estimated by the UT and the MCM. (d) Absolute difference between the relative uncertainties estimated by the UT and the MCM.

irradiance is 0.125 %.

Fig. 8a and 8c show that the uncertainties derived with the GUF and the UT follow with good agreement those of the MCM. Specifically, the absolute difference between the two methods and the MCM is virtually identical and increases steadily from −3.8E-5 % at 290 nm to −3.04E-5 % at 363 nm. Moreover, the mean relative difference is −3.39E-5 %. Therefore, this confirms that the GUF and the UT accurately estimate the lamp current component of the combined standard uncertainty.

#### 4.2.6. *Distance*

The uncertainty produced in UV measurements by the distance adjustment has no dependence on wavelength or solar zenith angle. The MCM estimates it as 0.23885 %, the UT as 0.23891 %, and the GUF as 0.23875 %. Therefore, the relative difference between the GUF and the MCM is less than 0.09 %, while the difference between the UT and the MCM is less than 0.03 %.

#### 4.2.7. *Radiometric stability*

The relative uncertainty caused by the radiometric instability decreases with wavelength, ranging from 3.9 % at 290 nm to 3.3 % at 363 nm (see Fig. 9a and 9c). Therefore, the stability of the instrument is the source that contributes most to the uncertainty budget of Brewer #150 UV measurements. In fact, it represents more than 80 % of the combined standard uncertainty for wavelengths larger than 302 nm (see Sect. 4.2.11).

As seen in Fig. 9a and 9c the three methodologies provide similar estimations for this uncertainty source. In particular, the UT method marginally underestimates this contribution with an average absolute difference that increases from −0.018 % at 295 nm to −0.013 % at 360 nm (see Fig. 9d). The GUF also underestimates slightly this contribution with an average difference that varies between −0.02 % at 295 nm and −0.015 % at 360 nm. Furthermore, the relative difference between the two methods and the MCM is less than 0.49 % for the GUF and 0.43 % for all wavelengths measured. Consequently, the GUF and UT approaches provide accurate values of the stability component of the combined standard UV uncertainty.

The radiometric instability is larger for Brewer #150 than for other double-monochromator instruments. For example, the instability is of the order of 0.6 % for the QASUME unit [45], 0.4 % for the Bentham DTMc300 with serial number 5541 [31], or 1.5 % at 350 nm for the IFU spectroradiometer [12]. However, Garane et al. [34] found that the radiometric stability was ~ 2.8 % and ~ 3.3 % for Brewers #086 (type MKIII) and #005 (type MKII), respectively. This could indicate that Brewer spectrometers are more affected by the instability of their photomultiplier tubes (PMT) than other spectroradiometers.

#### 4.2.8. *Temperature correction*

Fig. 10a and 10c illustrate that the uncertainty caused by the temperature correction has no spectral dependency. This was expected since the correction factor for Brewer #150 also displays this behaviour [37]. However, the temperature contribution does depend on the SZA, increasing from 0.04 % at a SZA of 32° to 0.15 % at a SZA of 61°. As SZA grows and Sun altitude declines, the temperature of the instrument decreases. As a result, the difference between the Brewer temperature and the reference (33 °C) increases and, in turn, the temperature correction becomes more important, as shown in Eq. (11).

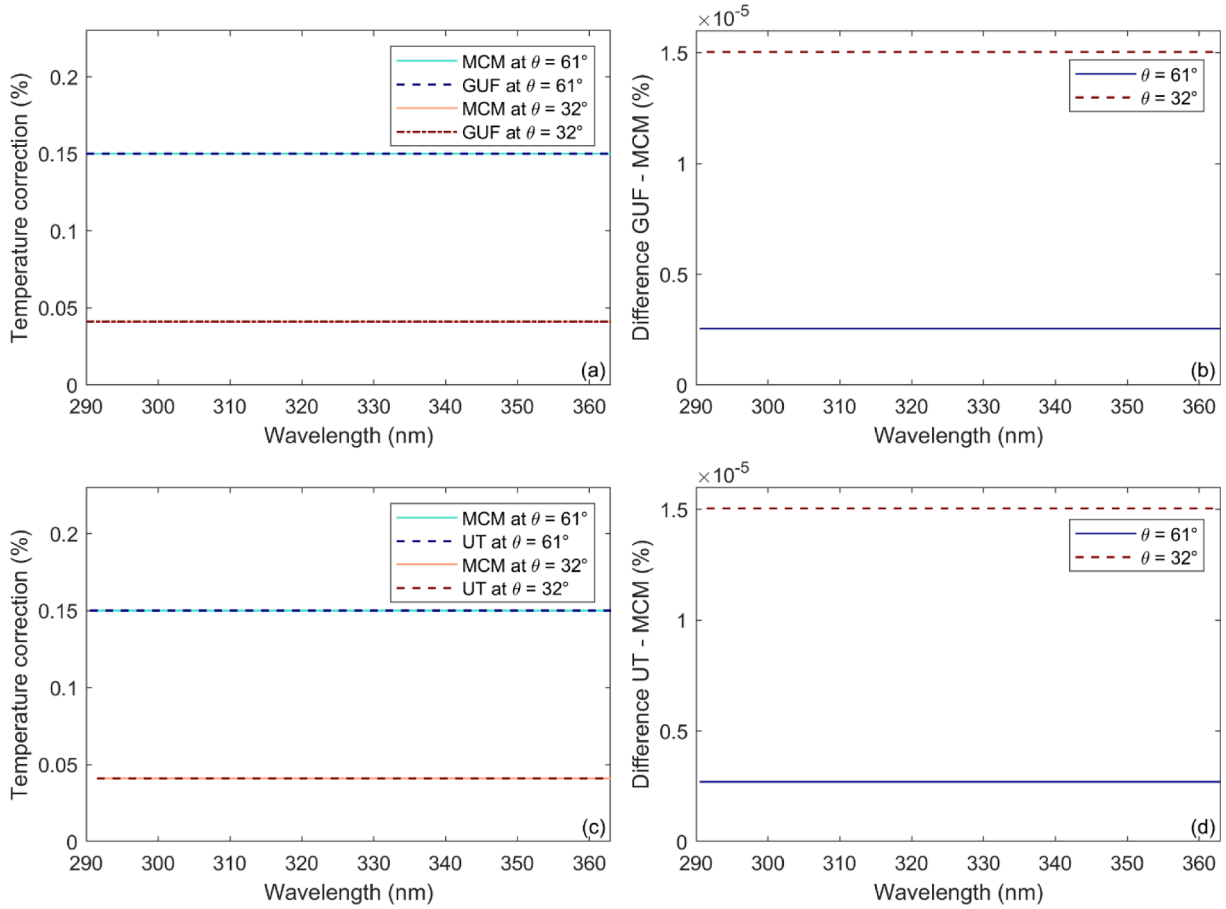



**Fig. 10.** Comparison of MCM, UT, and GUF estimations of the uncertainty produced by the temperature correction. (a) MCM and GUF relative spectral uncertainties caused by the temperature correction. (b) Absolute difference between the relative uncertainties estimated by the GUF and the MCM. (c) MCM and UT relative spectral uncertainties caused by the temperature correction. (d) Absolute difference between the relative uncertainties estimated by the UT and the MCM.

The GUF accurately reproduces the uncertainties derived from the MCM (Fig. 10a). The absolute difference between the two methods declines slightly with increasing SZA (see Fig. 10b), from 1.5E-5 % at 32° SZA to 2.5E-6 % at 61° SZA. The corresponding relative differences are 0.04 % at 32° and 0.0017 % at 61°. Similar results are obtained for the UT technique. The absolute difference between the UT and the MCM rises with SZA (as shown in Fig. 10d), from 2.7E-6 % at 61° SZA to 1.5E-5 % at 32° SZA. This results in relative differences of 0.04 % at 32° and 0.0018 % at 61° SZA. The differences between the three methodologies are virtually zero since the temperature correction is an input variable with a clear Gaussian PDF and, moreover, its sensitivity coefficient is easy to calculate.

#### 4.2.9. *Cosine correction*

Fig. 11a and 11c show that the uncertainties due to the cosine correction of Brewer #150 UV data depend significantly on both SZA and wavelength. For 61° SZA this component decreases gradually from 0.44 % at 300 nm to 0.35 % at 360 nm. For 32° SZA, it increases slightly from 0.41 % at 300 nm to 0.45 % at 360 nm. Consequently, the cosine correction is one of the error sources that contributes most to the uncertainty of Brewer global UV measurements (see Sect. 4.2.11). For the UVA region and a SZA of 61°, cosine correction is the fourth most important uncertainty source, after stability, lamp spectral irradiance, and noise.

Although the absolute difference between the GUF and the MCM is spectrally dependent, it varies less than ± 0.01 %, for the SZAs recorded. On average, the GUF slightly underestimates this contribution as the mean difference with the MCM was −0.002 % and −0.01 % at 61° and 32° SZA, respectively. Regarding the UT, its difference with the MCM also depends on wavelength, especially at large SZAs. Overall, the UT slightly overestimates this source as the mean difference with the MCM was, on average, 0.002 % at 61° and 9E-5 % at 32°.

#### 4.2.10. *Wavelength misalignment*

Fig. 12a and 12 d illustrate that the relative uncertainty arising from wavelength misalignment depends on both wavelength and SZA. It decreases steadily between 290 and 310 nm. At larger wavelengths, above 310 nm, the relative uncertainty levels off at around 0.21 % at 61° and 0.12 % at 32°. Therefore, the influence of this error source increases with SZA.

Furthermore, Fig. 12 also shows that both the UT and the GUF methodologies overestimate the MCM uncertainties as SZA increases. This effect is more marked at short wavelengths, below 300 nm. For this wavelength region and at a SZA of 61°, the absolute difference GUF-MCM is 0.68 % and the UT-MCM is 0.58 %. As wavelength increases, above 310 nm, the absolute difference GUF-MCM levels off at 0.41 % at 61° SZA and 0.06 % at 32° SZA. These discrepancies were expected since the two methods estimated differently the wavelength shift contribution. For the GUF approach, it was determined using a radiative transfer model as the partial derivation was a challenging task. On the other hand, the MCM estimated this contribution by modifying the wavelength scale according to the wavelength shifts $\Delta\lambda$. As for the UT-MCM, for wavelengths above 310 nm it levels off at 0.14 % at 61° SZA and 0.03 % at 32° SZA. Therefore, its estimations are more accurate than those provided by the GUF. This was also expected, since the wavelength shift was implemented in the UT following a methodology similar to the

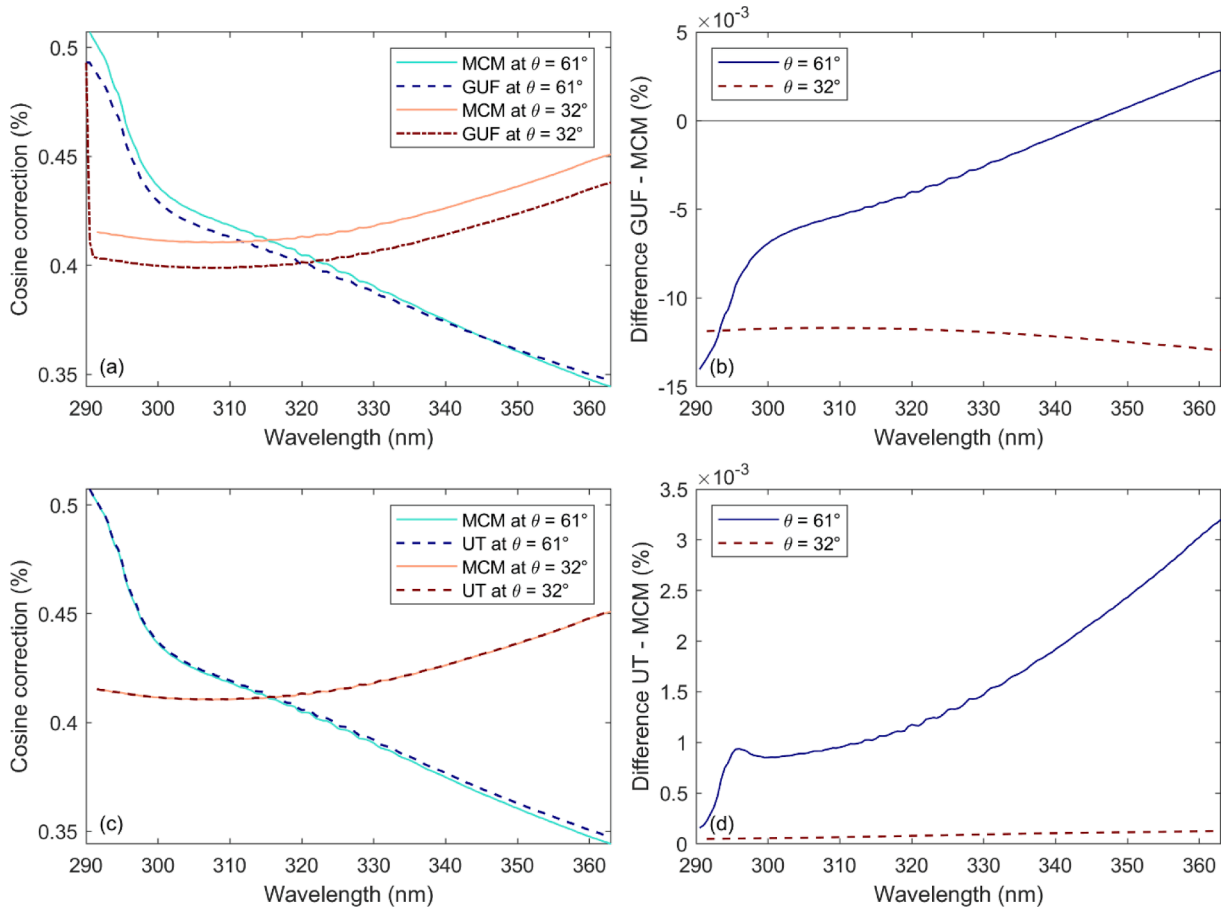



**Fig. 11.** Comparison of MCM, UT, and GUF estimations of the uncertainty produced by the cosine correction. (a) GUF and MCM relative spectral uncertainty caused by the cosine correction. (b) Absolute difference between the relative uncertainties estimated by the GUF and the MCM. (c) UT and MCM relative spectral uncertainty caused by the cosine correction. (d) Absolute difference between the relative uncertainties estimated by the UT and the MCM.

one used in the MCM, i.e. modifying the wavelength scale using the sigma points (previously defined with the wavelength shifts). Nevertheless, the GUF methodology provides satisfactory estimations for this contribution as well.

#### 4.2.11. *Summary of the sensitivity analysis*

To identify the dominant uncertainty sources, the contributions of all error sources to the combined standard uncertainty are presented together in Fig. 13.

Fig. 13a shows that at short wavelengths (302 nm) and large SZAs the dominant sources are noise, radiometric stability, wavelength misalignment, and the irradiance of the reference lamp. This is similar to the results found for other double monochromator spectrometers [25,30,36]. For smaller SZAs (see Fig. 13b), as the irradiance signal increases, noise, and wavelength misalignment lose influence and the radiometric stability gains it. At wavelengths above 310 nm, the stability is the most dominant source, independently of the SZA. From the remaining sources, the most significant ones are the spectral irradiance of the reference lamp, the cosine correction, the noise, and dead time of the photomultiplier tube (PMT). Therefore, reducing the overall uncertainty of Brewer #150 would depend mostly on decreasing the instability and noise of the PMT. Noise could be reduced by increasing the duration of the UV scan. However, decreasing significantly the instability is harder to achieve as it implies changing the detector for other types of detection systems.

## 5. Conclusions

The GUM uncertainty framework (GUF) and the Unscented transformation (UT) have been validated against the Monte Carlo method (MCM) for the evaluation of the uncertainty of solar UV irradiance measurements. The spectra used were recorded by Brewer #150 during the XVI Intercomparison Campaign of the RBCC-E, from 10 to 15 September 2021.

To carry out the uncertainty evaluation, the error sources affecting Brewer UV measurements were characterised and the irradiance measurement model described. For the GUF approach, the non-linearity of the model was disregarded and the combined standard uncertainty was obtained using the law of propagation of uncertainties. As for the UT, the uncertainty analysis was carried out by defining a small set of sigma points and propagating them through the non-linear irradiance model. Regarding the MCM, it was implemented through a simulation that calculated the UV irradiance many times (4E6 trials) while varying the error sources according to their PDFs (gaussian or rectangular).

The comparison between the MCM, the UT, and the GUF methods for the estimation of the combined standard uncertainty showed that the GUF and UT methodologies provides reliable estimations. The mean ratio between the GUF and the MCM for the 290–363 nm region was 1.008 and 0.992 for a SZA of 61° and 32°, respectively. Moreover, the relative difference between the two methods was less than 2 % for wavelengths above 320 nm and SZAs below 65°. As for the UT, its mean ratio to the MCM for the 290–363 nm was 1.001 at 61° SZA and 1.003 at 32° SZA. Consequently, the UT provides more accurate estimations than the GUF for the uncertainty evaluation of spectral UV irradiance.

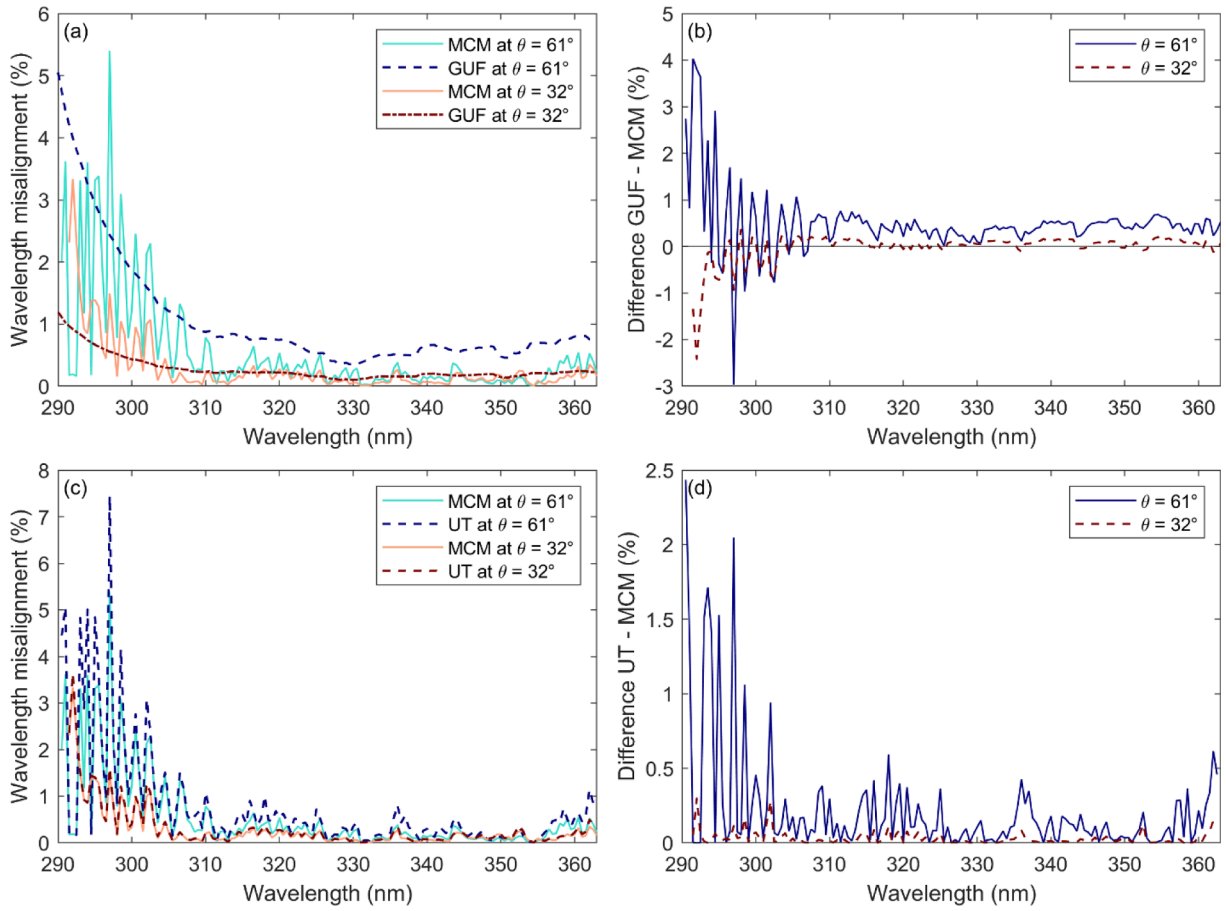



**Fig. 12.** Comparison of MCM, UT, and GUF estimations of the uncertainty produced by the wavelength misalignment of the spectroradiometer at two SZAs, 32° and 61°. (a) GUF and MCM relative spectral uncertainty caused by wavelength misalignment. (b) Absolute difference between the relative uncertainties estimated by the GUF and the MCM. (c) UT and MCM relative spectral uncertainty produced by wavelength misalignment. (d) Absolute difference between the estimations of the UT and the MCM.

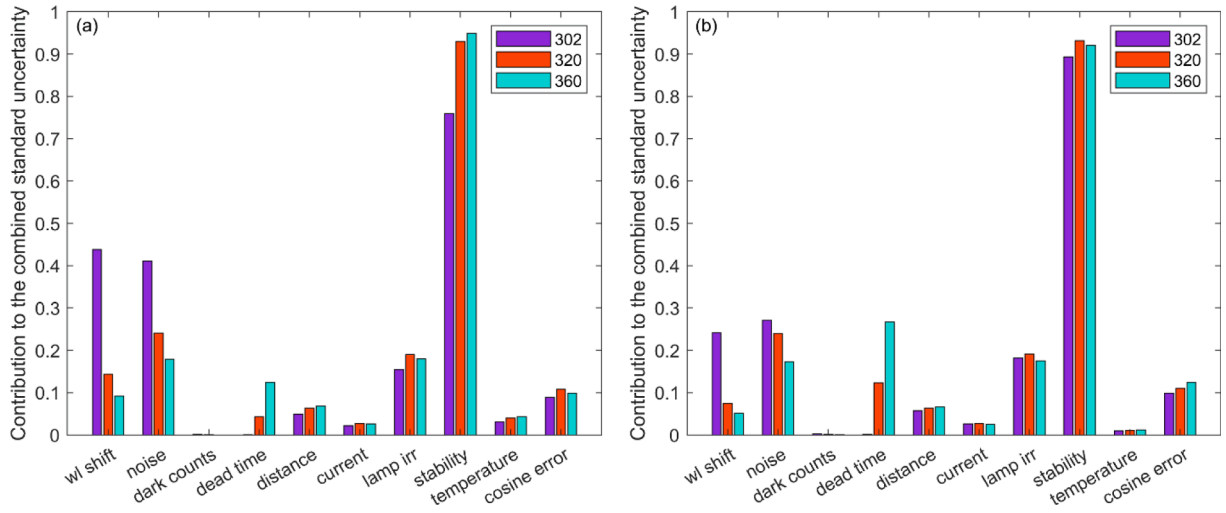



**Fig. 13.** Contribution of the ten uncertainty sources considered in the study to the combined standard uncertainty of the UV spectrum measured on 10 September 2021 at three wavelengths (302, 320, and 360 nm) and two SZAs, (a) 61° and (b) 32°.

Although the irradiance model is clearly non-linear, assuming liner effects in the uncertainty propagation resulted in reliable uncertainty estimations (the ratio GUF/MCM was stable and close to unity). Non-linear effects could be masked because there is a dominant uncertainty source in Brewer UV measurements. To check this hypothesis, the uncertainty evaluation was performed without considering the radiometric stability, the error source that contributes the most to the uncertainty budget. The resulting average ratio between the GUF and the MCM was 1.111 at 61° and 0.976 at 32° SZA. Furthermore, the relative difference was 12.5 % at 61° and 3.0 % at 32° SZA for wavelengths

larger than 320 nm. Consequently, the discrepancy between the two methods increased considerably, especially at large SZAs, above 60°. On the other hand, the ratio between the UT and the MCM was 1.019 at 61° and 1.007 at 32°. This translates into relative differences, for wavelengths above 320 nm of 1.79 % and 0.53 % at 61° and 32° SZA, respectively. Therefore, these results indicate that the UV uncertainties estimated by the GUF might be unreliable if the error sources affecting the measurement contribute equally to the uncertainty budget. In these cases, the UT is a suitable alternative, as its estimations were similar to those of the MCM, with a relative difference of less than 2 % with the MCM.

The sensitivity analysis showed that at short wavelengths the most important sources of uncertainty are noise, radiometric stability, and wavelength misalignment. However, at longer wavelengths, above 300 nm, the radiometric stability, dead time, the irradiance of the reference lamp, and the cosine error become important. In fact, the instability of Brewer #150 is the most important source of error for wavelengths above 300 nm. Therefore, reducing the combined standard uncertainty of Brewer #150 UV measurements could be achieved by calibrating the instrument more frequently, thus decreasing its instability. Nevertheless, a substantial reduction could require greater effects, such as replacing the PMT with other types of detection systems. This experiment was carried out by Hülsen et al. [36] for the QASUME spectrometer. They developed a new unit, QASUMEII, that uses a solid-state detection system instead of the traditional PMT. This resulted in a reduction of the stability, from 0.6 % to 0.2 %.

Furthermore, the GUF and UT estimate satisfactorily the contribution of every error source to the total uncertainty budget, i.e. the sensitivity analysis of both methodologies is accurate. In fact, the maximum relative differences between the MCM and the GUF were less than 3 % for all uncertainty sources except dead time and wavelength shift. For these two sources, the difference with the MCM increased due to the complexity of the propagation of their uncertainties. Nevertheless, the differences between the GUF and the MCM were, for these two sources, less than 10 % for all wavelengths measured and SZAs below 65°. On the other hand, the maximum relative differences between the MCM and the UT were less than 2.5 % for all uncertainty sources. Unlike the GUF, the UT reproduced correctly the influence of wavelength shift on the total irradiance uncertainty. As a result, its sensitivity analysis was more accurate than the one from the GUF.

It should be noted that the methods used for the uncertainty evaluation (MCM, UT, and GUF) are general and have been implemented following the recommendations set by the GUM. The uncertainty sources considered are common for all spectroradiometers measuring spectral UV irradiance. As a result, the analytical method developed, the Monte Carlo simulation, and the Unscented transformation implemented in this study can be easily adapted to other spectroradiometers provided they are characterised first (the code containing the uncertainty calculation for Brewer #150 is available on Zenodo). For single monochromators, like CCD-array spectroradiometers, it could be harder to adapt the methodology used since the stray light has not been included in the uncertainty analysis (it is negligible for double monochromator instruments like Brewer #150). Nonetheless, the characterisation and the effect of stray light on the uncertainty have already been analysed in other studies (e.g. [78–80]).

## CRediT authorship contribution statement

**Carmen González:** Writing – original draft, Visualization, Validation, Software, Methodology, Investigation, Formal analysis, Data curation, Conceptualization. **José M. Vilaplana:** Writing – review & editing, Validation, Supervision, Resources, Methodology, Investigation, Funding acquisition, Conceptualization. **Francisco C. Parra-Rojas:** Writing – review & editing, Validation, Supervision, Methodology, Formal analysis. **Antonio Serrano:** Writing – review & editing, Validation, Supervision, Software, Resources, Methodology, Investigation, Data curation, Conceptualization.

## Data availability

The dataset used for the uncertainty evaluation of Brewer #150 is available at Zenodo [81]. The software (version 2.0) associated with this manuscript for the implementation of the GUM uncertainty framework, Unscented transformation, and Monte Carlo method is published on Zenodo [82]. Ozone data measured by Brewer #150 was used in the creation of this manuscript and can be downloaded from EuBrewNet [83]. Aerosol optical depth measured at INTA/El Arenosillo station was used for the cosine correction and can be downloaded from AERONET [84,85]. For the calculation of solar UV radiation in the Earth's atmosphere the libRadtran radiative transfer model was used [71].

## Declaration of competing interest

The authors declare that they have no known competing financial interests or personal relationships that could have appeared to influence the work reported in this paper.

## Acknowledgments

The authors declare that they have no conflict of interest. This work was supported by MCIN/AEI/10.13039/501100011033 and "European Union NextGenerationEU/PRTR" [Grant TED2021-130532A-I00]; and by ESA-MPC, Aemet [KNMI- Contract Number 2020/658, 2020].

We also thank Victoria E. Cachorro Revilla and Margarita Yela González for their effort in establishing and maintaining AERONET El Arenosillo/Huelva site.

## References

[1] K.H. Kaidbey, A.M. Kligman, The acute effects of long-wave ultraviolet radiation on human skin, J, Invest. Dermatol. 72 (5) (1979) 253–256, https://doi.org/10.1111/1523-1747.ep12531710.
[2] M. Norval, G.M. Halliday, The consequences of UV-induced immunosuppression for human health, Photochem. Photobiol. 87 (5) (2011) 965–977, https://doi.org/10.1111/j.1751-1097.2011.00969.x.
[3] G.H. Bernhard, R.E. Neale, P.W. Barnes, P.J. Neale, R.G. Zepp, S.R. Wilson, A. L. Andrady, A.F. Bais, R.L. McKenzie, P.J. Aucamp, P.J. Young, J.B. Liley, R. M. Lucas, S. Yazar, L.E. Rhodes, S.N. Byrne, L.M. Hollestein, C.M. Olsen, A. R. Young, C.C. White, Environmental effects of stratospheric ozone depletion, UV radiation and interactions with climate change: UNEP environmental effects assessment panel, update 2019, Photochem. Photobiol. Sci. 19 (5) (2020) 542–584, https://doi.org/10.1039/d0 pp90011g.
[4] A.R. Wegener, In vivo studies on the effect of UV-radiation on the eye lens in animals, Doc. Ophthalmol. 88 (3–4) (1995) 221–232, https://doi.org/10.1007/BF01203676.
[5] M.M. Caldwell, L.O. Björn, J.F. Bornman, S.D. Flint, G. Kulandaivelu, A. H. Teramura, M. Tevini, Effects of increased solar ultraviolet radiation on terrestrial ecosystems, J. Photochem. Photobiol. B Biol. 46 (1–3) (1998) 40–52, https://doi.org/10.1016/S1011-1344(98)00184-5.
[6] H.B. Ozel, A.E.S. Abo Aisha, M. Cetin, H. Sevik, I. Zeren Cetin, The effects of increased exposure time to UV-B radiation on germination and seedling development of Anatolian black pine seeds, Environm. Monitor. Assessm. 193 (7) (2021), https://doi.org/10.1007/s10661-021-09178-9.
[7] A.H. Teramura, Effects of ultraviolet-B radiation on the growth and yield of crop plants, Physiol. Plant. 58 (3) (1983) 415–427, https://doi.org/10.1111/j.1399-3054.1983.tb04203.x.
[8] J.C. Chang, S.F. Ossoff, D.C. Lobe, M.H. Dorfman, C.M. Dumais, R.G. Qualls, J. D. Johnson, UV inactivation of pathogenic and indicator microorganisms, Appl. Environ. Microbiol. 49 (6) (1985) 1361–1365, https://doi.org/10.1128/aem.49.6.1361-1365.1985.
[9] N. Giese, J. Darby, Sensitivity of microorganisms to different wavelengths of UV light: implications on modeling of medium pressure UV systems, Water Res. 34 (16) (2000) 4007–4013, https://doi.org/10.1016/S0043-1354(00)00172-X.
[10] G.D. Harris, V.D. Adams, D.L. Sorensen, M.S. Curtis, Ultraviolet inactivation of selected bacteria and viruses with photoreactivation of the bacteria, Water Res. 21 (6) (1987) 687–692, https://doi.org/10.1016/0043-1354(87)90080-7.
[11] G. Kelfkens, F.R. de Gruijl, J.C. van der Leun, Ozone depletion and increase in annual carcinogenic ultraviolet dose, Photochem. Photobiol. 52 (4) (1990) 819–823, https://doi.org/10.1111/j.1751-1097.1990.tb08687.x.
[12] J.B. Kerr, C.T. McElroy, Evidence for large upward trends of ultraviolet-B radiation linked to ozone depletion, Science 262 (5136) (1993) 1032–1034, https://doi.org/10.1126/science.262.5136.1032.

[13] V.E. Fioletov, L.J.B. McArthur, J.B. Kerr, D.I. Wardle, Long-term variations of UV-B irradiance over Canada estimated from Brewer observations and derived from ozone and pyranometer measurements, J. Geophys. Res. Atmos. 106 (D19) (2001) 23009–23027, https://doi.org/10.1029/2001JD000367.
[14] K. Lakkala, E. Kyrö, T. Turunen, Spectral UV measurements at Sodankylä during 1990–2001, J. Geophys. Res. Atmos. 108 (19) (2003), https://doi.org/10.1029/2002jd003300.
[15] A.F. Bais, A. Kazantzidis, S. Kazadzis, D.S. Balis, C.S. Zerefos, C. Meleti, Deriving an effective aerosol single scattering albedo from spectral surface UV irradiance measurements, Atmos. Environ. 39 (6) (2005) 1093–1102, https://doi.org/10.1016/j.atmosenv.2004.09.080.
[16] N. Siomos, I. Fountoulakis, A. Natsis, T. Drosoglou, A. Bais, Automated Aerosol Classification from Spectral UV Measurements Using Machine Learning Clustering, Remote Sens. (Basel) 12 (6) (2020) 965, https://doi.org/10.3390/rs12060965.
[17] A.F. Bais, C.S. Zerefos, C. Meleti, I.C. Ziomas, K. Tourpali, Spectral measurements of solar UVB radiation and its relations to total ozone, $SO_2$, and clouds, J. Geophys. Res. Atmos. 98 (D3) (1993) 5199–5204, https://doi.org/10.1029/92JD02904.
[18] K. Stamnes, J. Slusser, M. Bowen, Derivation of total ozone abundance and cloud effects from spectral irradiance measurements, Appl. Opt. 30 (30) (1991) 4418–4426, https://doi.org/10.1364/AO.30.004418.
[19] A. Cede, J. Herman, A. Richter, N. Krotkov, J. Burrows, Measurements of nitrogen dioxide total column amounts using a Brewer double spectrophotometer in direct Sun mode, J. Geophys. Res. Atmos. 111 (D5) (2006), https://doi.org/10.1029/2005JD006585.
[20] J.B. Kerr, C.T. McElroy, Total ozone measurements made with the Brewer ozone spectrophotometer during STOIC 1989, J. Geophys. Res. Atmos. 100 (D5) (1995) 9225–9230, https://doi.org/10.1029/94JD02147.
[21] A.F. Bais, B.G. Gardiner, H. Slaper, M. Blumthaler, G. Bernhard, R. McKenzie, A. R. Webb, G. Seckmeyer, B. Kjeldstad, T. Koskela, P.J. Kirsch, J. Gröbner, J.B. Kerr, S. Kazadzis, K. Leszczynski, D. Wardle, W. Josefsson, C. Brogniez, D. Gillotay, A. Redondas, SUSPEN intercomparison of ultraviolet spectroradiometers, J. Geophys. Res. Atmos. 106 (D12) (2001) 12509–12525, https://doi.org/10.1029/2000JD900561.
[22] L. Egli, J. Gröbner, G. Hülsen, L. Bachmann, M. Blumthaler, J. Dubard, M. Khazova, R. Kift, K. Hoogendijk, A. Serrano, A. Smedley, J.-M. Vilaplana, Quality assessment of solar UV irradiance measured with array spectroradiometers, Atmos. Meas. Tech. 9 (4) (2016) 1553–1567, https://doi.org/10.5194/amt-9-1553-2016.
[23] K. Lakkala, A. Arola, J. Gröbner, S.F. León-Luis, A. Redondas, S. Kazadzis, T. Karppinen, J.M. Karhu, L. Egli, A. Heikkilä, T. Koskela, A. Serrano, J. M. Vilaplana, Performance of the FMI cosine error correction method for the Brewer spectral UV measurements, Atmos. Meas. Tech. 11 (9) (2018) 5167–5180, https://doi.org/10.5194/amt-11-5167-2018.
[24] BIPM, IEC, IFCC, ISO, IUPAC, IUPAP & OIML. (2008a). Evaluation of Measurement Data – Guide to the Expression of Uncertainty in Measurement. Bureau International des Poids et Mesures, JCGM 100.
[25] G. Bernhard, G. Seckmeyer, Uncertainty of measurements of spectral solar UV irradiance, J. Geophys. Res. Atmos. 104 (D12) (1999) 14321–14345, https://doi.org/10.1029/1999JD900180.
[26] G. Seckmeyer, A. Bais, G. Bernhard, M. Blumthaler, C. Booth, P. Disterhoft, P. Eriksen, R. McKenzie, M. Miyauchi, C. Roy. Instruments to measure solar ultraviolet irradiance. Part 1: Spectral instruments (GAW Report No. 125). World Meteorological Organization (WMO) (2001).
[27] A.R. Webb, B.G. Gardiner, T.J. Martin, K. Leszcynski, J. Metzdorf, V.A. Mohnen. Guidelines for Site Quality Control of UV Monitoring (GAW Report No. 126). World Meteorological Organization (WMO) (1998).
[28] I. Fountoulakis, H. Diémoz, A.M. Siani, G. Hülsen, J. Gröbner, Monitoring of solar spectral ultraviolet irradiance in Aosta Italy, Earth Syst. Sic. Data 12 (4) (2020) 2787–2810, https://doi.org/10.5194/essd-12-2787-2020.
[29] K. Garane, A.F. Bais, S. Kazadzis, A. Kazantzidis, C. Meleti, Monitoring of UV spectral irradiance at Thessaloniki (1990–2005): Data re-evaluation and quality control, Ann. Geophys. 24 (12) (2006) 3215–3228, https://doi.org/10.5194/angeo-24-3215-2006.
[30] J. Gröbner, J. Schreder, S. Kazadzis, A.F. Bais, M. Blumthaler, P. Görts, R. Tax, T. Koskela, G. Seckmeyer, A.R. Webb, D. Rembges, Traveling reference spectroradiometer for routine quality assurance of spectral solar ultraviolet irradiance measurements, Appl. Opt. 44 (25) (2005) 5321–5331, https://doi.org/10.1364/AO.44.005321.
[31] N. Kouremeti, A. Bais, S. Kazadzis, M. Blumthaler, R. Schmitt, Charge-coupled device spectrograph for direct solar irradiance and sky radiance measurements, Appl. Opt. 47 (10) (2008) 1594–1607, https://doi.org/10.1364/AO.47.001594.
[32] K. Lakkala, A. Arola, A. Heikkilä, J. Kaurola, T. Koskela, E. Kyrö, A. Lindfors, O. Meinander, A. Tanskanen, J. Gröbner, G. Hülsen, Quality assurance of the Brewer spectral UV measurements in Finland, Atmos. Chem. Phys. 8 (13) (2008) 3369–3383, https://doi.org/10.5194/acp-8-3369-2008.
[33] C. González, J.M. Vilaplana, A. Serrano, Monte Carlo Evaluation of Uncertainties of UV Spectra Measured With Brewer Spectroradiometers, J. Geophys. Res. Atmos. 128 (24) (2023), https://doi.org/10.1029/2023JD039500.
[34] A.F. Bais, Spectrometers: Operational Errors and Uncertainties, in: C.S. Zerefos, A. F. Bais (Eds.), Solar Ultraviolet Radiation. NATO ASI Series, vol 52, Springer, Berlin, Heidelberg, 1997, https://doi.org/10.1007/978-3-662-03375-3_12.
[35] J. Gröbner, P. Sperfeld, Direct traceability of the portable QASUME irradiance scale to the primary irradiance standard of the PTB, Metrologia 42 (2) (2005) 134–139, https://doi.org/10.1088/0026-1394/42/2/008.
[36] G. Hülsen, J. Gröbner, S. Nevas, P. Sperfeld, L. Egli, G. Porrovecchio, M. Smid, Traceability of solar UV measurements using the QASUME reference spectroradiometer, Appl. Opt. 55 (26) (2016) 7265–7275, https://doi.org/10.1364/ao.55.007265.
[37] BIPM, IEC, IFCC, ILAC, ISO, IUPAC, & OIML. (2008b). Evaluation of Measurement Data – Supplement 1 to the Guide to the Expression of Uncertainty in Measurement – Propagation of distributions using a Monte Carlo method. Bureau International des Poids et Mesures, JCGM 101.
[38] S.J. Julier. The scaled unscented transformation. Proceedings of the 2002 American Control Conference (IEEE Cat. No.CH37301) (2002), 4555–4559. doi: 10.1109/ACC.2002.1025369.
[39] L. Angrisani, M. D'Apuzzo, R. Schiano Lo Moriello. The unscented transform: a powerful tool for measurement uncertainty evaluation. Proceedings of the 2005 IEEE International Workshop OnAdvanced Methods for Uncertainty Estimation in Measurement, (2005), 27–32. doi: 10.1109/AMUEM.2005.1594599.
[40] D.A. Perez, H. Gietler, H. Zangl. Automatic Uncertainty Propagation Based on the Unscented Transform. 2020 IEEE International Instrumentation and Measurement Technology Conference (I2MTC) (2020), 1–6. doi: 10.1109/I2MTC43013.2020.9129581.
[41] C.M. Rocco Sanseverino, J.E. Ramirez-Marquez, Uncertainty propagation and sensitivity analysis in system reliability assessment via unscented transformation, Reliab. Eng. Syst. Saf. 132 (2014) 176–185, https://doi.org/10.1016/j.ress.2014.07.024.
[42] Y. Zhou, C. He, J. Li, J. Lin, L. Wei, Y Wang, Uncertainty analysis of vehicle-pedestrian accident reconstruction based on unscented transformation, Forensic Sci. Int. 342 (2023), https://doi.org/10.1016/j.forsciint.2022.111505.
[43] L. Wang, R. Ding, A parameter determination method of unscented transformation and its approximate ability analysis in the precision estimation of nonlinear measurement adjustment, Measurement 166 (2020), https://doi.org/10.1016/j.measurement.2020.108065.
[44] P. Kärhä, A. Vaskuri, H. Mäntynen, N. Mikkonen, E. Ikonen, Method for estimating effects of unknown correlations in spectral irradiance data on uncertainties of spectrally integrated colorimetric quantities, Metrologia 54 (4) (2017) 524–534, https://doi.org/10.1088/1681-7575/aa7b39.
[45] M. Antón, V.E. Cachorro, J.M. Vilaplana, C. Toledano, N.A. Krotkov, A. Arola, A. Serrano, B. De La Morena, Comparison of UV irradiances from Aura/Ozone Monitoring Instrument (OMI) with brewer measurements at El Arenosillo (Spain) – Part 1: analysis of parameter influence, Atmos. Chem. Phys. 10 (13) (2010) 5979–5989, https://doi.org/10.5194/acp-10-5979-2010.
[46] M. Antón, A. Serrano, M.L. Cancillo, J.M. Vilaplana, Quality assurance of broadband erythemal radiometers at the Extremadura UV Monitoring Network (Southwestern Spain), Atmos. Res. 100 (1) (2011) 83–92, https://doi.org/10.1016/j.atmosres.2010.12.029.
[47] M. Antón, A. Serrano, M.L. Cancillo, J.M. Vilaplana, V.E. Cachorro, J. Gröbner, Correction of angular response error in brewer UV irradiance measurements, J. Atmos. Oceanic Tech. 25 (11) (2008) 2018–2027, https://doi.org/10.1175/2008JTECHA1040.1.
[48] V.E. Cachorro, R. Vergaz, M.J. Martin, A.M. de Frutos, J.M. Vilaplana, B. de la Morena, Measurements and estimation of the columnar optical depth of tropospheric aerosols in the UV spectral region, Ann. Geophys. 20 (4) (2002) 565–574, https://doi.org/10.5194/angeo-20-565-2002.
[49] V.E. Cachorro, C. Toledano, M. Antón, A. Berjón, A. de Frutos, J.M. Vilaplana, A. Arola, N.A. Krotkov, Comparison of UV irradiances from Aura/Ozone Monitoring Instrument (OMI) with Brewer measurements at El Arenosillo (Spain) – Part 2: Analysis of site aerosol influence, Atmos. Chem. Phys. 10 (23) (2010) 11867–11880, https://doi.org/10.5194/acp-10-11867-2010.
[50] M.L. Cancillo, A. Serrano, M. Antón, J.A. García, J. Vilaplana, B. de la Morena, An improved outdoor calibration procedure for broadband ultraviolet radiometers, Photochem. Photobiol. 81 (4) (2005) 860–865, https://doi.org/10.1111/j.1751-1097.2005.tb01454.x.
[51] C. González, J.M. Vilaplana, J.A. Bogeat, A. Serrano, Comparison of global UV spectral irradiance measurements between a BTS CCD-array and a Brewer spectroradiometer, Atmos. Meas. Tech. 15 (13) (2022) 4125–4133, https://doi.org/10.5194/amt-15-4125-2022.
[52] P.G. Kosmopoulos, S. Kazadzis, A.W. Schmalwieser, P.I. Raptis, K. Papachristopoulou, I. Fountoulakis, A. Masoom, A.F. Bais, J. Bilbao, M. Blumthaler, A. Kreuter, A.M. Siani, K. Eleftheratos, C. Topaloglou, J. Gröbner, B. Johnsen, T.M. Svendby, J.M. Vilaplana, L. Doppler, C. Kontoes, Real-time UV index retrieval in Europe using Earth observation-based techniques: system description and quality assessment, Atmos. Meas. Tech. 14 (8) (2021) 5657–5699, https://doi.org/10.5194/amt-14-5657-2021.
[53] A.A. Piedehierro, M.L. Cancillo, A. Serrano, M. Antón, J.M. Vilaplana, Global irradiance calibration of multifilter UV radiometers, J. Geophys. Res. 121 (1) (2016) 427–438, https://doi.org/10.1002/2015JD023935.
[54] J. Gröbner, Improved entrance optic for global irradiance measurements with a Brewer spectrophotometer, Appl. Opt. 42 (18) (2003) 3516–3521, https://doi.org/10.1364/AO.42.003516.
[55] A.F. Bais, C.S. Zerefos, C.T. McElroy, Solar UVB measurements with the double- and single-monochromator Brewer ozone spectrophotometers, Geophys. Res. Lett. 23 (8) (1996) 833–836, https://doi.org/10.1029/96GL00842.
[56] J. Gröbner, M. Blumthaler, S. Kazadzis, A. Bais, A. Webb, J. Schreder, G. Seckmeyer, D. Rembges, Quality assurance of spectral solar UV measurements: results from 25 UV monitoring sites in Europe, 2002 to 2004, Metrologia 43 (2) (2006) S66–S71, https://doi.org/10.1088/0026-1394/43/2/S14.
[57] R.R. Cordero, G. Seckmeyer, S. Riechelmann, A. Damiani, F. Labbe, Monte carlo-based uncertainty analysis of UV array spectroradiometers, Metrologia 49 (6) (2012) 745–755, https://doi.org/10.1088/0026-1394/49/6/745.

[58] J.J. Davenport, J. Hodgkinson, J.R. Saffell, R.P. Tatam, Noise analysis for CCD-based ultraviolet and visible spectrophotometry, Appl. Opt. 54 (27) (2015) 8135–8144, https://doi.org/10.1364/ao.54.008135.
[59] I. Fountoulakis, A. Redondas, A.F. Bais, J.J. Rodriguez-Franco, K. Fragkos, A. Cede, Dead time effect on the Brewer measurements: Correction and estimated uncertainties, Atmos. Meas. Tech. 9 (4) (2016) 1799–1816, https://doi.org/10.5194/amt-9-1799-2016.
[60] A.R. Webb, B.G. Gardiner, M. Blumthaler, P. Forster, M. Huber, P.J. Kirsch, A laboratory investigation of two ultraviolet spectroradiometers, Photochem. Photobiol. 60 (1) (1994) 84–90, https://doi.org/10.1111/j.1751-1097.1994.tb03947.x.
[61] C. Schinke, H. Pollex, D. Hinken, M. Wolf, K. Bothe, I. Kröger, S. Nevas, S. Winter, Calibrating spectrometers for measurements of the spectral irradiance caused by solar radiation, Metrologia 57 (6) (2020) 065027, https://doi.org/10.1088/1681-7575/abafc5.
[62] R.W. Engstrom, Multiplier Photo-Tube Characteristics: Application to Low Light Levels*, J. Opt. Soc. Am. 37 (6) (1947) 420–431, https://doi.org/10.1364/JOSA.37.000420.
[63] I. Fountoulakis, A. Redondas, K. Lakkala, A. Berjon, A.F. Bais, L. Doppler, U. Feister, A. Heikkila, T. Karppinen, J.M. Karhu, T. Koskela, K. Garane, K. Fragkos, V. Savastiouk, Temperature dependence of the Brewer global UV measurements, Atmos. Meas. Tech. 10 (11) (2017) 4491–4505, https://doi.org/10.5194/amt-10-4491-2017.
[64] E. Weatherhead, D. Theisen, A. Stevermer, J. Enagonio, B. Rabinovitch, P. Disterhoft, K. Lantz, R. Meltzer, J. Sabburg, J. DeLuisi, J. Rives, J. Shreffler, Temperature dependence of the Brewer ultraviolet data, J. Geophys. Res. Atmosph. 106 (D24) (2001) 34121–34129, https://doi.org/10.1029/2001JD000625.
[65] A.F. Bais, S. Kazadzis, K. Garane, N. Kouremeti, J. Gröbner, M. Blumthaler, G. Seckmeyer, A.R. Webb, T. Koskela, P. Görts, J. Schreder, Portable device for characterizing the angular response of UV spectroradiometers, Appl. Opt. 44 (33) (2005) 7136–7143, https://doi.org/10.1364/AO.44.007136.
[66] A.F. Bais, S. Kazadzis, D. Balis, C.S. Zerefos, M Blumthaler, Correcting global solar ultraviolet spectra recorded by a Brewer spectroradiometer for its angular response error, Appl. Opt. 37 (27) (1998) 6339–6344, https://doi.org/10.1364/AO.37.006339.
[67] M. Blumthaler, J. Gröbner, M. Huber, W. Ambach, Measuring spectral and spatial variations of UVA and UVB sky radiance, Geophys. Res. Lett. 23 (5) (1996) 547–550, https://doi.org/10.1029/96GL00248.
[68] V.E. Fioletov, J.B. Kerr, D.I. Wardle, N.A. Krotkov, J.R. Herman, Comparison of Brewer ultraviolet irradiance measurements with total ozone mapping spectrometer satellite retrievals, Opt. Eng. 41 (12) (2002) 3051–3061, https://doi.org/10.1117/1.1516818.
[69] U. Feister, R. Grewe, K. Gericke, A method for correction of cosine errors in measurements of spectral UV irradiance, Sol. Energy 60 (6) (1997) 313–332, https://doi.org/10.1016/S0038-092X(97)00030-3.
[70] J. Gröbner, M. Blumthaler, W. Ambach, Experimental investigation of spectral global irradiance measurement errors due to a non ideal cosine response, Geophys. Res. Lett. 23 (18) (1996) 2493–2496, https://doi.org/10.1029/96GL02380.
[71] C. Emde, R. Buras-Schnell, A. Kylling, B. Mayer, J. Gasteiger, U. Hamann, J. Kylling, B. Richter, C. Pause, T. Dowling, L. Bugliaro, The libRadtran software package for radiative transfer calculations (version 2.0.1), Geosci. Model Dev. 9 (5) (2016) 1647–1672, https://doi.org/10.5194/gmd-9-1647-2016.
[72] B. Mayer, A. Kylling, Technical note: The libRadtran software package for radiative transfer calculations - description and examples of use, Atmos. Chem. Phys. 5 (7) (2005) 1855–1877, https://doi.org/10.5194/acp-5-1855-2005.
[73] H. Slaper, H.A.J.M. Reinen, M. Blumthaler, M. Huber, F. Kuik, Comparing ground-level spectrally resolved solar UV measurements using various instruments: A technique resolving effects of wavelength shift and slit width, Geophys. Res. Lett. 22 (20) (1995) 2721–2724, https://doi.org/10.1029/95GL02824.
[74] J. Gröbner, D.I. Wardle, C.T. McElroy, J.B. Kerr, Investigation of the wavelength accuracy of Brewer spectrophotometers, Appl. Opt. 37 (36) (1998) 8352–8360, https://doi.org/10.1364/AO.37.008352.
[75] E.A. Wan, R. van der Merwe. The unscented Kalman filter for nonlinear estimation. Proceedings of the IEEE 2000 Adaptive Systems for Signal Processing, Communications, and Control Symposium (2000), 153–158. doi: 10.1109/ASSPCC.2000.882463.
[76] R. Turner, C.E. Rasmussen, Model based learning of sigma points in unscented Kalman filtering, IEEE International Workshop on Machine Learning for Signal Processing 2010 (2010) 178–183, https://doi.org/10.1109/MLSP.2010.5589003.
[77] R.R. Cordero, G. Seckmeyer, D. Pissulla, L. Dasilva, F. Labbe, Uncertainty evaluation of spectral UV irradiance measurements, Meas. Sci. Technol. 19 (4) (2008), https://doi.org/10.1088/0957-0233/19/4/045104.
[78] S. Nevas, J. Gröbner, L. Egli, M. Blumthaler, Stray light correction of array spectroradiometers for solar UV measurements, Appl. Opt. 53 (19) (2014) 4313, https://doi.org/10.1364/AO.53.004313.
[79] C. Schinke, M. Franke, K. Bothe, S. Nevas, Implementation and uncertainty evaluation of spectral stray light correction by Zong's method, Appl. Opt. 58 (36) (2019) 9998, https://doi.org/10.1364/AO.58.009998.
[80] Y. Zong, S.W. Brown, B.C. Johnson, K.R. Lykke, Y. Ohno, Simple spectral stray light correction method for array spectroradiometers, Appl. Opt. 45 (6) (2006) 1111, https://doi.org/10.1364/AO.45.001111.
[81] C. González, J.M. Vilaplana, F.C. Parra-Rojas, A. Serrano, UV scans measured by Brewer #150 during the XVI intercomparison campaign of the RBCC-E and their associated uncertainties [Data set]. Zenodo. https://doi.org/10.5281/zenodo.12790731.
[82] C. González, J.M. Vilaplana, F.C. Parra-Rojas, A. Serrano, GUM uncertainty framework, Unscented transformation, and Monte Carlo approaches for the uncertainty evaluation of Brewer UV measurements (Version 2.0) [Software]. Zenodo. https://doi.org/10.5281/zenodo.12790742.
[83] J.S. Rimmer, A. Redondas, T. Karppinen, EuBrewNet – A European Brewer network (COST Action ES1207), an overview, Atmos. Chem. Phys. 18 (14) (2018) 10347–10353. doi:10.5194/acp-18-10347-2018.
[84] O. Dubovik, M. D. King, A flexible inversion algorithm for retrieval of aerosol optical properties from Sun and sky radiance measurements. J. Geophys. Res. Atmosph. *105*(D16) (2000) 20673–20696. doi:10.1029/2000JD900282.
[85] B. N. Holben, T.F. Eck, I. Slutsker, D. Tanré, J.P. Buis, A. Setzer, E. Vermote, J. A. Reagan, Y.J. Kaufman, T. Nakajima, F. Lavenu, I. Jankowiak, A. Smirnov, AERONET—A Federated Instrument Network and Data Archive for Aerosol Characterization, Remote Sensing of Environment 66 (1) (1998) 1–16. doi:10.1016/S0034-4257(98)00031-5.